Nanoconstructs for Advances in Photodynamic Therapy

By

Thomas Hopkins

A dissertation submitted in partial fulfillment
of the requirements for the degree of
Doctor of Philosophy
(Chemistry)
in The University of Michigan
2018

Doctoral Committee:

Professor Raoul Kopelman, Chair
Professor Julie Biteen
Professor Theodore Goodson III
Professor Xueding Wang

Thomas J. J. Hopkins

TJJH@umich.edu

ORCID iD: 0000-0002-5613-3449

To my family who supported me over the years through my own thick and thin decisions

Acknowledgments

I would like to first recognize and thank my mentor, Professor Raoul Kopelman, for his guidance and attention over the years. When I first entered his lab in winter of 2014, I had no experience, let alone knowledge, of the work, challenges, and on-going collaborations in the biomedical research field towards cancer diagnosis and therapy. This has provided me with unique experience in having to operate in an area with well defined, but difficult to manipulate parameters and systems, cultivating an important facet for any good scientist: thinking outside of the box.

I would also like to thank my committee members Drs. Julie Biteen, Xueding Wang, and Theodore Goodson III for their guidance and substantial advice in completing my PhD.

Further, I would like to extend this recognition to the members of the Kopelman lab and associated collaborators, who often sat down to explore new ideas and critique existing ones, leading to the rapid advances of each other's projects.

Table of Contents

List of Figures

List of Tables

Abstract

Nanoparticle (NP) based systems have advanced the efficacy of treating cancer by enabling selective accumulation of drugs in tumors. Photodynamic therapy (PDT) is an exceptionally promising modality for its triple selectivity in treating cancer: requiring light, oxygen, and a photosensitizer (PS). The choice of a PS can become important not only for its absorption spectrum but also its relative aggression in causing oxidative stress; clinicians may prefer one PS over another depending on the type of response required to elicit optimal treatment. We show in Chapter 2 using polyacrylamide (PAAm) hydrogel NPs that chlorin e6 (Ce6) is a much more aggressive PDT agent than the classically applied methylene blue (MB). In addition to understanding the relative aggression of a PS in PDT, design of the NP is important to optimizing both the reactive oxygen species (ROS) producing capabilities and the means of effective delivery. Previously reported 8-arm polyethylene glycol amine (8PEGA) has been used to stop heart arrhythmia via PDT from conjugated Ce6. This NP is ideal for also targeting cancer due to the optimized ROS production, ease of changing targets, and its small size that would allow for deep tumor penetration *in vivo*. In Chapter 3, the tumor targeting peptide F3-cys was successfully grafted to 8PEGA-Ce6 and cancer cells efficiently ablated *in vitro*, demonstrating promise in translation to cancer *in vivo*. In addition, 8PEGA was shown to be a very promising diffusion weighted magnetic resonance (MR) imaging agent for cancer due to its long T_2 lifetime and high molecular weight. 8PEGA may then potentially act as an efficient agent in MR of tumors *in vivo* without the use of toxic heavy metal atoms. Lastly, while NP-mediated PDT has been efficiently described in treating cancer and stopping heart arrhythmia, it may also be

suitable to treating cancer-like diseases, such as choroidal neovascularization (CNV). In Chapter 4, the FDA-approved dyes indocyanine green (ICG) and the PS verteporfin (VP) were successfully encapsulated in pluronic micelles and shown to ablate cancer cells with low inherent toxicity. Given the cancer-like nature of CNV, NP-mediated PDT looks like a potential modality for treatment. The presented systems are effective in evaluation of their objectives and should further encourage clinical adoption of NPs for theranostics (PDT + imaging) by being simple to prepare, purify, and exceptionally biocompatible.

Chapter 1: Introduction

1.1 A brief history of PDT

Photodynamic therapy (PDT) is the process by which biological material is ablated via oxidative stress. The first evidence of this process was reported by a Dr. Hermann von Tappeiner of Germany when attempting to treat various skin conditions using light. He observed that a combination of a photosensitizer (PS), oxygen, and light would yield a reaction in the skin conditions, which he later coined "photodynamic action" in 1904.[1]

In 1948, Figge and co. discovered that porphyrin dyes (a class of dyes known to be PSs) had an affinity for accumulating in rapidly dividing cells.[2] Based on this, the hypothesis that PDT could be used to treat cancer began to take substantial shape within the scientific community. Thomas Dougherty and co. of the Rosewell Park Cancer Institute clinically tested PDT in 1978, where they showed substantial success in their preliminary work; 111 of 113 malignant tumors tested displayed either total or partial resolution.[3] The dye employed by Dougherty, known as HpD, became the first clinically approved dye for PDT in 1993, under the brand name Photofrin, for treatment of bladder cancer in Canada. Their work was essentially limited to near surface tumors, where visible photons are not significantly absorbed or scattered.

In more recent years, a substantial degree of effort has been put towards refining the PDT methodology for non-superficial application.[4] PDT has shown great promise using Photofrin, but there remains substantial work to be done in reconciling this modality against the inherent problems of tumors in biological models (e.g. non-specific PS interactions with blood proteins, tissue hypoxia, lack of active PS targeting).[3]

1.2 Inherent Problems of Dyes in PDT

The first and most apparent problem in the viable application of PDT *in vivo* is the lack of targetability and stability of dyes suitable to function as PSs. PSs chosen for use *in vivo* are non-toxic in the absence of light, but do not naturally accumulate in tumor cells, are rapidly scavenged by the immune system, and in some cases, such as methylene blue's, are reduced in the blood, resulting in their loss of photodynamic activity.[5,6]

Photosensitizers have been attached directly to targeting agents (peptides[7,8] and antibodies[9,10]) that are tooled to bind and enter specific cells. This is advantageous as a general application for PSs by: 1) triggering cell uptake of a PS and 2) causing the uptake of a PS to be selective towards cancer cells. However, this method is not viable for PSs, such as methylene blue,[11] that are susceptible to reduction by blood enzymes. This method is further complicated by a need to preserve the structure of a targeting agent when modifying it, to maintain its cell specificity, and the difficulty in purifying targeted materials of free PS. In addition, antibodies specifically are exceptionally expensive, and so those alone do not represent an economically viable application of PDT. Nanoparticle (NP) based systems therefore represent a more viable method of delivery of PSs for cancer PDT *in vivo*.

1.3 Nanoparticles as Solutions of Inherent Problems in PDT

One of the earliest engineered NPs was reported by the Kopelman lab, where it was shown that NPs (coined as nano-PEBBLES at the time) can function as efficient vehicles for delivery of dyes to cells for a variety of applications.[12] This pioneering work was later extended for cell-targeted PDT in cancer.[5,13] Shortly thereafter, it was also shown that using these NP-

based systems offered the advantage of protecting the PS methylene blue from blood enzyme reduction, indicating that NPs are capable of protecting a PSs photoactivity in a biological environment.[6] Following the initial work using silica and polyacrylamide (PAAm) based PEBBLES in the Kopelman lab, a wide range and variety of NPs have been produced and tested for delivery of a PS, such as: silica gel,[14] poly-(lactic-co-glycolic acid),[15] keratin,[16] self-assembled proteins,[17] and noble metal NPs.[18]

Silica gel can be considered the classical example of NPs in PDT application due to being the earliest known report.[5] Silica gel is a highly stable material, resistant to breakdown in biological systems, and may efficiently encapsulate a PS during synthesis.[13] However, silica gel is also a very dense material, offering little in the way of porosity, inherently leading to lower PDT viability by limiting oxygen diffusion within the matrix.[13] These limitations have been improved upon by generating meso-porous silica gel nanoparticles, leading to significantly better oxygen diffusion and thus PDT performance.[19] However, silica gel NPs suffer from low renal clearance kinetics due to their stability.[20] NPs more likely to be FDA-approved would ideally decompose more quickly in the filtration organs.

PAAm hydrogel is the succeeding material to silica gel in targeted NP-PDT. These NPs are simple to prepare, purify, and may be loaded with any PS one may desire at necessary concentrations.[6] Additionally, covalent linkage and encapsulation leads to increased photo-stability by limiting solvent effects and preventing dye aggregation/leakage. These NPs are also composed of crosslinkers that enable their controlled biodegradation, allowing for significantly quicker body clearance.[21,22] Polyacrylamide displays superior PDT efficacy when compared to silica gel due to being significantly more porous.[13] It represents the first material to accomplish targeted PDT that may be non-superficially applied to animals.

Noble metal nanoparticles, specifically gold, have also been examined as vehicles for PDT. Gold is generally considered to be a non-toxic substance, has a well understood surface chemistry for modification, and may enhance PDT properties of a PS.[23] Gold (Au) NPs may also renally clear the body efficiently if engineered correctly.[24] However, AuNPs are limited purely to their surfaces in terms of modification, meaning that there is a significant limit to the amount of PS that may be loaded, and the PS used may not be segregated from the local biological environment. In addition, AuNPs can be efficient fluorescence quenchers, and thus if not engineered carefully will diminish or prevent PDT.[23]

8-arm polyethylene glycol amine (8PEGA) has also been successfully used as a nanocarrier in PDT for the stopping of heart arrhythmia by ablating cardio-myocytes.[25] It was shown that the attachment of the PS chlorin e6 (Ce6) to 8PEGA significantly improved PDT efficacy by 50% when compared to the free PS.[26] The 8PEGA was also shown to be targetable, cell-selective, and capable of penetrating dense tissue due to its small hydrodynamic volume. Additionally, though this has yet to be explored, its small size may allow for rapid renal clearance. However, the small size may yet present a challenge in cancer application due to tumors having a positive pressure, known to prevent significant entry of chemodrugs.[27]

Clearly, there are limits and advantages to using certain NP constructions. This should be expected however, as different biological conditions will necessitate meeting different requirements. There should not be any NP construction thought of as ‘universal’, though it would not be unlikely to see constructions that can be applied to multiple situations.

In addition to the transport of PSs for delivery to cancer cells, NPs also benefit from the enhanced retention and permeability (EPR) effect, where they tend to accumulate within the tumor area due to its anomalous vasculature.[27]

NPs thus have the tendency to enable the protected delivery of a PS to a cancer cell for PDT, preserve its photoactivity by excluding PS interactions with the blood enzymes, and by extension, increase its blood circulation time *in vivo*. However, this still leaves the issue of targeting, a two-fold issue.

The first issue with NPs is that without any targeting, they, like the PSs, hold no affinity to any specific cell type. The second issue is that NPs will experience non-specific protein adsorption to their surface (surface fouling), resulting in a loss of blood circulation time due to scavenging by blood macrophages and immune cells (though they do overall represent a net increase in blood circulation time for the PS than without the NP present).[28] Both of these problems can be overcome by applying PEG.

PEG has been shown to be a very good substance for disguising NPs from the immune system and preventing surface biofouling.[29] NPs (silica, polymeric, and otherwise) are typically functionalized with various primary amine containing groups for the wide range of modification chemistry this allows. These can be used to graft linear PEG onto their surfaces, resulting in a substantial improvement of blood circulation time. Noble metal NPs may also be functionalized with PEG by taking advantage of their well understood surface chemistry. Additionally, linear PEG is available as a heterofunctional moiety, allowing for the other end that is not mounted to the NP surface to be used as a molecular anchor for targeting agents to the NPs.[30] Thus, NPs may be cell-specific targeted and achieve long blood circulation time, increasing the accumulation of a PS in the tumor area.

1.4 Biological Challenges in PDT Application

The above thus sufficiently addresses the first problems with achieving non-superficial (effective and cell-selective) application of cancer PDT *in vivo*. The second issue to be addressed is maximizing the efficacy of PDT. This is critical because advanced tumors are hypoxic in nature.[31] PDT relies on the destruction of cancer cells via oxidative stress produced by reactive oxygen species (ROS), resulting through reaction with the local oxygen; thus, it becomes especially important that PDT is applied in such a way as to maximize its effects.[32] The relative hypoxia of a tumor based on distance from vasculature as a result of proliferation is shown in Figure 1-1.[33]

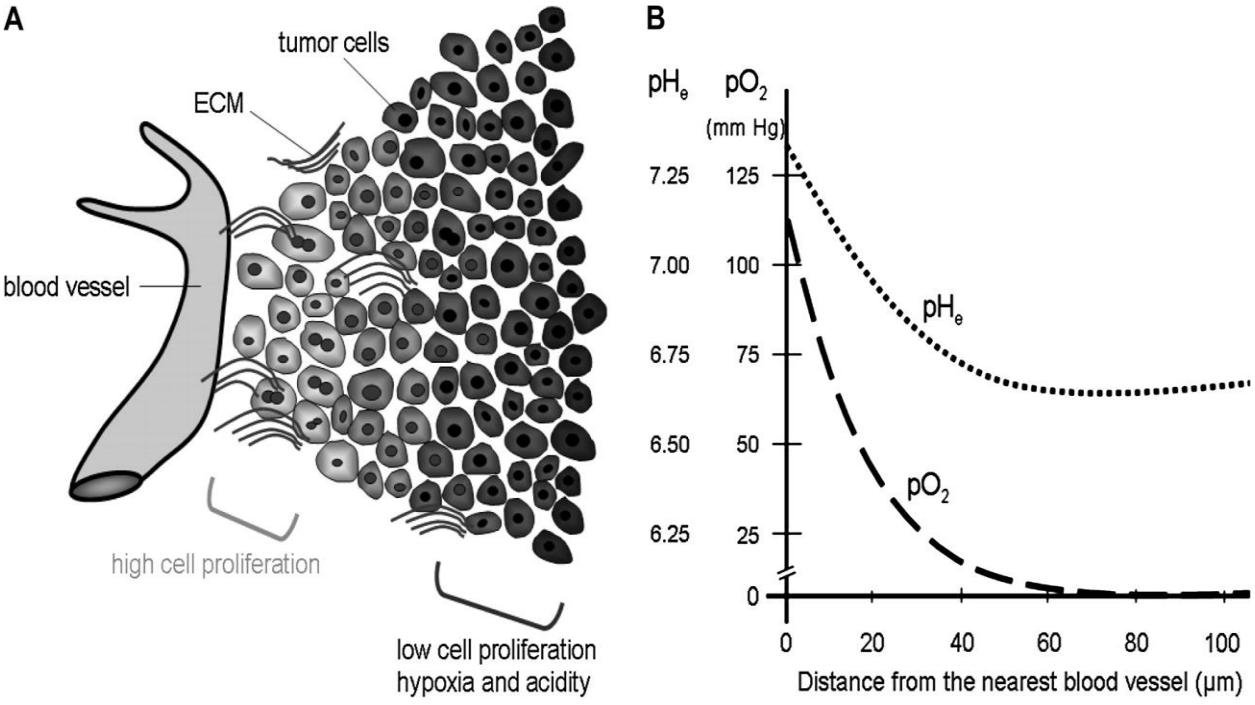

Figure 1-1: Tumor hypoxia as a result of unchecked tissue growth. A) Cartoon of tumor cell proliferation with respect to vasculature proximity. B) Quantification of tumor oxygenation with respect to vasculature proximity; Dotted line = extracellular pH, Dashed = tumor oxygenation. Reproduced from reference 33.

As was explored before, a PS is encapsulated in NPs to protect them during delivery to the sites of interest for a given application. This will lead to a decrease in ROS production over the free dye because oxygen must diffuse into the housing matrix and ROS diffuse out without attacking that matrix. One method of maximizing this ROS production is to tailor the NP matrix to be especially porous.[34] This leads to more efficient usage of the ROS, enabling greater efficacy in a hypoxic environment.

Another explored method is to drag oxygen into the tumor cells by using nanodroplets of perfluoronated materials. Perfluorocarbons (PFC) are biologically safe materials that have exceptional oxygen solvation properties and so are desirable to be incorporated into NPs, whereby they may mediate the PDT, avoiding reliance upon the biologically present oxygen.[35] Unfortunately, a majority of PFCs are hydrophobic, limiting their applications in biological systems. Micelles or liposomes make excellent carriers for hydrophobic materials, allowing for their dispersion in aqueous media. A phospholipid that incorporates perfluorohexane into its core as a nanodroplet has been recently reported where it increased both radiation therapy and PDT efficacy.[36,37]

Thus, hypoxia in tumors can be addressed as a PDT limitation through suitable synthetic designs and material choices. The final limitation that must be considered when applying PDT to a tumor is its physiology. In its most basic form, a tumor can be described as a de-regulated growth of a cell population. Under such conditions, they will eventually approach the point of nutrient deficiency. When this point is reached, there are two possible outcomes: angiogenesis or cells switching to anaerobic glycolysis.[38-40]

For the cells that undergo anaerobic glycolysis, they will eventually die as tumor progress leads to further nutrient deficiencies. However, the tissue that experiences angiogenesis to form

new leaky vasculatures will support the continued growth of cancerous tissue. NPs take advantage of the leaky nature in the cancerous vasculature through the EPR effect to accumulate.[41,42] Since the coining of angiogenesis in 1971, it has largely been assumed that tumors grow exclusively through this method. As a result, vascular targeted PDT (VPDT) has become a topic of focus in treating cancer.[43,44]

However, it has recently been reported that tumor growth is supported by a combination of angiogenesis and healthy vasculatures.[45,46] This raises the problem of NPs being able to adequately treat certain types of cancer that may have low angiogenic expression. To our knowledge, no work has been done towards expressly exploring this, making exploration appealing for: 1) evaluating how NP systems must change to ensure tissue penetration and 2) re-evaluate the depth to which hypoxia may fluctuate and affect PDT efficacy.[47]

Irrespective of the anomalous nature of tumor structuring, like any healthy tissue it may limit optical transparency. This can be overcome to a certain extent by designing fiber optic systems that allow for adequate illumination of PSs to initiate PDT treatment,[48] but it is always desirable to use long wavelength, near infrared active dye moieties, due to the greatly reduced tissue light scattering and absorption in these spectral regimes.

The greatest tissue penetration of light capable of exciting molecular electronic transitions for ROS production occurs at what is known as the first optical window, ranging from 650 – 950nm (Figure 1-2).[49,50]

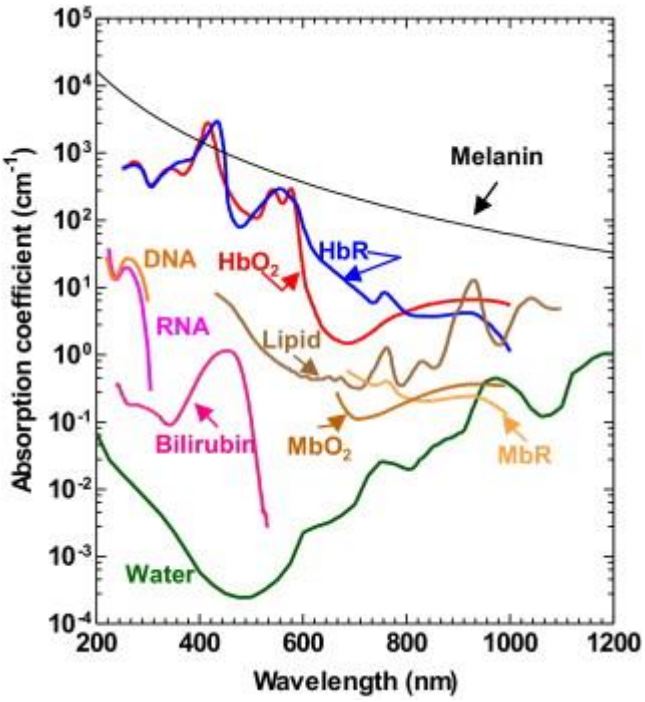

Figure 1-2: Various contributions to optical density by tissue in vivo. HbO2 = oxy-hemoglobin, HbR = deoxy-hemoglobin, MbO2 = oxy-myoglobin, MbR = deoxy-myoglobin. Reproduced from reference 50.

There is a severe lack of dyes that efficiently produce ROS with absorption located in this range. Indocyanine green (ICG) and NIR783 have been shown to be capable of PDT but require high laser powers due to their low ROS production.[51,52] Another method of realizing deeper penetrating PDT is the use of upconverting nanocrystals.[53,54] However, upconverting nanocrystals are typically made of rare-earth materials and suffer from low brightness (causing low PDT viability).[55]

1.5 Overview of Dissertation

The aforementioned topics clearly show that PDT is a highly viable method of controlled and precise cancer ablation, owing to its four-fold selectivity (requires light, oxygen, PS, and can

be targeted using NPs with peptides/antibodies). However, to realize a successful extension of PDT to subsurface tumors in the clinical setting there is still much work to be done in refining designs towards such applications.

While design of NP matrices is important to the evaluation of systems for viable PDT, the choice of PS also plays a significant role. Unfortunately, there is no library of data that thoroughly evaluates the relative efficacy of PSs in NP-PDT. Therefore, Chapter 2 places emphasis on investigating relative PDT effectiveness of two commonly employed PSs: methylene blue and chlorin e6. Both PSs are encapsulated in PAAm hydrogel NPs and their relative effectiveness at ablating cancer cells under identical illumination conditions are compared when correlated against their absorption properties.

In Chapter 3, the focus of the work is primarily on development of a peptide-polymer-PS conjugate, F3-8PEGA-Ce6, that is suitable for deep penetration of cancerous tissue, optimization of ROS production, and efficacy as an magnetic resonance (MR) imaging agent. The ROS production was compared against the traditional PS encapsulated PAAm model. Penetration of dense tissue with 8PEGA-Ce6 has previously been reported,[25] and the successful modification of the nanoplatform with another targeting agent indicates extension of application for 8PEGA-Ce6 as a whole to other biological areas of interest for PDT.

Lastly, while cancer has been the focus of this discussion, there do exist other biological abnormalities and conditions that resemble cancer to a remarkable degree, such as choroidal neovascularization (CNV). There are currently no cures for CNV, but there does exist an FDA-approved procedure of PDT.[56] However, a lack of cell specificity can cause severe side effects (secondary CNV or coronal atrophy),[56] and almost no literature exists on refining this. Chapter 4 therefore focuses on the refinement of PDT for CNV to suitably treat the condition by

encapsulating the FDA-approved dyes Verteporfin and ICG in micelles, testing their PDT efficacy and toxicity towards significantly improved cell specificity in CNV oriented PDT.

1.6 References

[1]Sharma, S.K.; Mroz, P.; Dai, T.; Huang, Y.; Denis, T.G.St.; Hamblin, M.R. Photodynamic Therapy for Cancer and for Infections: What Is the Difference? *Isr. J. Chem.*, 2012, **52**, 691 – 705. DOI: 10.1002/ijch.201100062.

[2]Figge F.H.J.; Weiland, G.S.; Manganiello, L.O.J. Cancer detection and therapy; affinity of neoplastic, embryonic, and traumatized tissues for porphyrins and metalloporphyrins. *Proc. Soc. Exp. Biol. Med.*, 1948, **68**, 640.

[3]Dougherty, T.J.; Kaufman, J.E.; Goldfarb, A.; Weishaupt, K.R.; Boyle, D.; Mittleman, A. Photoradiation therapy for treatment of malignant tumors. *Cancer Res.*, 1978, **38**, 2628 – 35.

[4]Lucky, S.S.; Soo, K.C.; Zhang, Y. Nanoparticles in Photodynamic Therapy. *Chem. Rev.*, 2015, **115**, 1990 – 2042. DOI: 10.1021/cr5004198.

[5]Yan, F.; Kopelman, R. The embedding of meta-tetra(hydroxyphenyl)-chlorin into silica nanoparticle platforms for photodynamic therapy and their singlet oxygen production and pH-dependent optical properties. *Photochem. Photobiol.*, 2003, **78**, 587 – 91.

[6]Kopelman et al. Multifunctional nanoparticle platforms for in vivo MRI enhancement and photodynamic therapy of a rat brain cancer. *J. Magn. Magn. Mater.*, 2005, **293**, 404 – 10.

[7]Kamarulzaman et al. New Peptide-Conjugated Chlorin-Type Photosensitizer Targeting Neuopilin-1 for Anti-Vascular Targeted Photodynamic Therapy. *Int. J. Mol. Sci.*, 2015, **16**, 24059 – 80. DOI: 10.3390/ijms161024059.

[8]Watanabe, K.; Fujiwara, H.; Kitamatsu, M.; Ohtsuki, T. Photoinduced apoptosis using a peptide carrying a photosensitizer. *Bioorganic Med. Chem. Lett.* 2016, **26**, 3115 – 8. DOI: 10.1016/j.bmcl.206.04.091.

[9]Pereira, P.M.; Korask, B.; Sarmento, B.; Schneider, R.J.; Fernandes, R.; Tome, J.P. Antibodies armed with photosensitizers: from chemical synthesis to photobiological applications. *Org. Biomol. Chem.*, 2015, **13**, 2518 – 29. DOI: 10.1039/C4OB02334J.

[10]Van Dongen, G.A.; Visser, G.W.; Vrouenraets, M.B. Photosensitizer-antibody conjugates for detection and therapy of cancer. *Adv. Drug Deliv. Rev.*, 2004, **13**, 31 – 52.

[11]Gibbs, W.N. The methylene blue reduction test: evaluation of a screening method for glucose-6-phosphate dehydrogenase deficiency. *Am. J. Trop. Med. Hyg.*, 1974, **23**, 1197 – 202.

[12]Clark, H.A.; Hoyer, M.; Philbert, M.A.; Kopelman, R. Optical nanosensors for chemical analysis inside single living cells. 1. Fabrication, characterization, and method for intracellular delivery of PEBBLE sensors. *Anal. Chem.*, 1999, **71**, 4831 – 6.

[13]Tang, W.; Xu, H.; Kopelman, R.; Philbert, M.A. Photodynamic Characterization and *In Vitro* Application of Methylene Blue-containing Nanoparticle Platforms. *Photochem. Photobiol.*, 2005, **81**, 242 – 9.

[14]Wang, Z.; Hong, X.; Zong, S.; Tang, C.; Cui, Y.; Zheng, Q. BODIPY-doped silica nanoparticles with reduced dye leakage and enhanced singlet oxygen generation. *Sci. Rep.*, 2015, **5**. DOI: 10.1038/srep12602.

[15]Ricci-Junior, E.; Marchetti, J.M. Zinc(II) pthalocyanine loaded PLGA nanoparticles for photodynamic therapy use. *Int. J. Pharm.*, 2006, **310**, 187 – 95. DOI: 10.1016/j.ijpharm.2005.10.048.

[16]Aluigi et al. Chlorin e6 keratin nanoparticles for photodynamic anticancer therapy. *RSC Adv.*, 2016, **6**, 33910 – 8. DOI: 10.1039/c6ra04208b.

[17]Wang, K.; Zhang, Y.; Wang, J.; Yuan, A.; Sun, M.; Wu, J.; Hu, Y. Self-assembled IR780-loaded transferrin nanoparticles as an imaging, targeting and PDT/PTT agent for cancer therapy. *Sci. Rep.*, 2016, **6**. DOI: 10.1038/srep27421.

[18]Bhaumik, J.; Gogia, G.; Kirar, S.; Vijay, L.; Thakur, N.S.; Banerjee, U.C.; Laha, J.K. Bioinspired nanophotosensitizers: synthesis and characterization of porphyrin – noble metal nanoparticle conjugates. *New J. Chem.*, 2016, **40**, 724 – 31. DOI: 10.1039/c5nj02056e.

[19]Liu, H.; Yang, Y.; Wang, A.; Han, M.; Cui, W.; Li, J. Hyperbranched polyglycerol-Doped Mesoporous Silica Nanoparticles for One- and Two-Photon Activated Photodynamic Therapy. *Adv. Funct. Mater.*, 2016, **26** 2561 – 70. DOI: 10.1002/adfm.201504939.

[20]Lee, J.A.; Kim, M.K.; Paek, H.J.; Kim, Y.R.; Kim, M.K.; Lee, J.K.; Jeong, J.; Choi, S.J. Tissue distribution and excretion kinetics of orally administered silica nanoparticles in rats. *Int. J. Nanomedicine*, 2014, **9**, 251 – 60. DOI: 10.2147/ijn.s57939.

[21]Wang, S.; Kim, G.; Lee, Y.E.; Hah, H.J.; Ethirajan, M.; Pandey, R.K.; Kopelman, R. Multifunctional Biodegradable Polyacrylamide Nanocarriers for Cancer Theranostics – A "See and Treat" Strategy. *ACS Nano*, 2012, **6**, 6843 – 51. DOI: 10.1021/nn301633m.

[22]Koo, Y.E.; Reddy, G.R.; Bhojani, M.; Schneider, R.; Philbert, M.A.; Rehemtulla, A.; Ross, B.D.; Kopelman, R. Brain Cancer Diagnosis and Therapy with Nanoplatforms. *Adv. Drug Deliv. Rev.*, 2006, **58**, 1556 – 77.

[23]Gamaleia, N.F.; Shton, I.O. Gold mining for PDT: Great expectations from tiny nanoparticles. *Photodiagnosis Photodyn. Ther.*, 2015, **12**, 221 – 31. DOI: 10.1016/j.pdpdt.2015.03.002.

[24]Xu, J.; Peng, C.; Yu, M.; Zheng, J. Renal clearable noble metal nanoparticles: photoluminescence, elimination, and biomedical applications. *Wiley Interdiscip. Rev. Nanomed. Nanobiotechnol.*, 2017, **9**. DOI: 10.1002/wnan.1453.

[25]Avula et al. Cell-selective arrhythmia ablation for photomodulation of heart rhythm. *Sci. Transl. Med.*, 2015, **7**, 311ra172. DOI: 10.1126/scitranslmed.aab3665.

[26]Lunt, S.J.; Fyles, A.; Hill, R.P.; Milosevic, M. Interstitial fluid pressure in tumors: therapeutic barrier and biomarker of angiogenesis. *Future Oncol.*, 2008, **4**, 793 – 802. DOI: 10.2217/14796694.4.6.793.

[27]Kobayashi, H.; Watanabe, R.; Choyke, P.L. Improving Conventional Enhanced Permeability and Retention (EPR) Effects; What Is the Appropriate Target? *Theranostics*, 2014, **4**, 81 – 9. DOI: 10.7150/thno.7193.

[28]Larson, T.A.; Joshi, P.P.; Sokolov, K. Preventing Protein Adsorption and Macrophage Uptake of Gold Nanoparticles *via* a Hydrophobic Shield. *ACS Nano*, 2012, **6**, 9182 – 90. DOI: 10.1021/nn3035155.

[29]Cruje, C.; Chithrani, D.B. Polyethylene Glycol Density and Length Affects Nanoparticle Uptake by Cancer Cells. *J. Nanomed. Res.*, 2014, **1**, 6. DOI: 10.15406/jnmr.2014.01.00006.

[30]Qin, M.; Hah, H.J.; Kim, G.; Nie, G.; Lee, Y.E.; Kopelman, R. Methylene blue covalently loaded polyacrylamide nanoparticles for enhanced tumor-targeted photodynamic therapy. *Photochem. Photobio. Sci.*, 2011, **10**, 832. DOI: 10.1039/c1pp05022b.

[31]Brown, J.M. Tumor hypoxia in cancer therapy. *Methods Enzymol.*, 2007, **435**, 297 – 321.

[32]Dabrowski, J.M. Chapter 9 – Reactice Oxygen Species in Photodynamic Therapy: Mechanisms of Their Generation and Potentitation. *Adv. Inorg. Chem.*, 2017, **70**, 343 – 94. DOI: 10.1016/bs.adioch.2017.03.002.

[33]Tredan, O.; Galmarini, C.M.; Patel, K.; Tannock, I.F. Drug Resistance and the Solid Tumor Microenvironment. *J. Natl. Cancer Inst.*, 2007, **99**, 1441 – 54. DOI: 10.1093/jnci/djm135.

[34]Yoon, H.K.; Lou, X.; Lee, Y.K.; Yoon, E.; Kopelman, R. Nano-photosensitizers Engineered to Generate a Tunable Mix of Reactive Oxygen Species, for Optimizing Photodynamic Therapy, Using a Microfluidic Device. *Chem. Mater.*, 2014, **26**, 1592 – 1600. DOI: 10.1021/cm403505s.

[35]Spahn, D.R. Blood substitutes Artificial oxygen carriers: perfluorocarbon emulsions. *Crit. Care*, 1999, **3**, R93 – 97.

[36]Xu, L.; Qiu, X.; Zhang, Y.; Cao, K.; Zhao, X.; Wu, J.; Hu, Y.; Guo, H. Liposome encapsulated perfluorohexane enhances radiotherapy in mice without additional oxygen supply. *Transl. Med.*, 2016, **14**, 268. DOI: 10.1186/s12967-016-1033-3.

[37]Cheng, Y.; Cheng, H.; Jiang, C.; Qiu, X.; Wang, K.; Huan, W. Yuan, A.; Wu, J.; Hu, Y. Perfluorocarbon nanoparticles enhance reactive oxygen levels and tumor growth inhibition in photodynamic therapy. *Nat. Commun.*, 2015, **6**, 8785. DOI: 10.1038/ncomms9785.

[38]Dhup, S.; Dadhich, R.K.; Porporato, P.E.; Sonveaux, P. Multiple biological activities of lactic acid in cancer: influences on tumor growth, angiogenesis and metastasis. *Curr. Pharm. Des.*, 2012, **18**, 1319 – 30.

[39]Folkman, J. Tumor Angiogenesis: Therapeutic Implications. *N. Engl. J. Med.*, 1971, **285**, 1182 – 6.

[40]Eales, K.L.; Hollinshead, K.E.; Tennant, D.A. Hypoxia and metabolic adaptation of cancer cells. *Oncongenesis*, 2016, **5**, e190. DOI: 10.1038/oncsis.2015.50.

[41]Podduturi, V.P.; Magana, I.B.; O'Neal, D.P.; Derosa, P.A. Simulation of transport and extravasation of nanoparticles in tumors which exhibit enhanced permeability and retention

effect. *Comput. Methods Programs Biomed.*, 2013, **112**, 58 – 68. DOI: 10.1016/j.cmpb.2013.06.011.

[42]Ho, Y.T.; Adriani, G.; Beyer, S.; Nhan, P.; Kamm, R.D.; Kah, J.C.Y. A Facile Method to Probe the Vascular Permeability of Nanoparticles in Nanomedicine Applications. *Sci Rep.*, 2017, **7**. DOI: 10.1038/s41598-017-00750-3.

[43]Leport, H. Vascular Targeted Photodynamic Therapy for Localized Prostate Cancer. *Rev. Urol.*, 2008, **10**, 254 – 61.

[44]Reddy et al. Vascular Targeted Nanoparticle for Imaging and Treatment of Brain Tumors. *Clin. Cancer. Res.*, 2006, **12**, 6677 – 86.

[45]Pezzella, F.; Gatter, K. Non-angiogenic tumours unveil a new chapter in cancer biology. *J. Pathol.*, 2015, **234**, 381 – 3. DOI: 10.1002/path.4474.

[46]Pezzella, F.; Gatter, K.C. Evidence Showing That Tumors Can Grow Without Angiogenesis and Can Switch Between Angiogenic and Nonangiogenic Phenotypes. *J. Natl. Cancer Inst.*, 2016, **108**. DOI: 10.1093/jnci/djw032.

[47]Chauhan, V.P.; Stylianopoulos, T.; Martin, J.D.; Popovic, Z; Chen, O.; Kamoun, W.S.; Bawendi, M.G.; Fukumura, D.; Jain, R.K. Normalization of tumour blood vessels improves the delivery of nanomedicines in size-dependent manner. *Nat. Nanotechnol.*, 2012, **7**, 383 – 88. DOI: 10.1038/nnao.2012.45.

[48]Agostinis et al. PHOTODYNAMIC THERAPY OF CANCER: AN UPDATE. *CA Cancer J. Clin.*, 2011, **61**, 250 – 81. DOI: 10.3322/caac.20114.

[49]Sordillo, L.A.; Pu, Y.; Pratavieria, S.; Budansky, Y.; Alfano, R.R. Deep optical imaging of tissue using the second and third near-infrared spectral windows. *J. Biomed. Opt.*, 2014, **19**. DOI: 10.1117/1.JBO.19.5.056004.

[50]Yao J.; Wang L.V. Sensitivity of photoacoustic microscopy. *Photoacoustics*. 2014, **2**, 87 – 101. DOI: 10.1016/j.pacs.2014.04.002.

[51]El-Daly, S.M.; Gamal-Eldeen, A.M.; Abo-Zeid, M.A.; Borai, I.H.; Wafay, H.A.; Abdel-Ghaffar, A.R. Photodynamic therapeutic activity of indocyanine green entrapped in polymeric nanoparticles. *Photodiagnosis Photodyn. Ther.*, 2013, **10**, 173 – 85. DOI: 10.1016/j.pdpdt.2012.08.003.

[52]Atchison et al. Iodinated Cyanine dyes: a new class of sensitizers for use in NIR activated photodynamic therapy (PDT). *Chem. Commun.*, 2017, **53**, 2009 – 12. DOI: 10.1039/c6cc09624g.

[53]Wang, C.; Cheng, L.; Liu, Z. Upconversion Nanoparticles for Photodynamic Therapy and Other Cancer Therapeutics. *Theranostics*, 2013, **3**, 317 – 30. DOI: 10.7150/thno.5284.

[54]Idris, N.M.; Gnanasammandhan, M.K.; Zhang, J.; Ho, P.C.; Mahendran, R.; Zhang, Y. *In vivo* photodynamic therapy using upconversion nanoparticles ass remote-controlled nanotransducers. *Nat. Med.*, 2012, **18**, 1580 – 5. DOI: 10.1038/nm.2933.

[55]Wilhelm, S. Perspectives for Upconverting Nanoparticles. *ACS Nano*, 2017, **11**, 10644 – 53. DOI: 10.1021/acsnano.7b07120.

[56]Newman, D.K. Photodynamic therapy: current role in the treatment of chorioretinal conditions. *Eye (Lond).*, 2016, **30**, 202 – 10. DOI: 10.1038/eye.2015.251.

Chapter 2: Intracellular Activity of Chlorin e6 Containing Nanoparticles

2.1 Introduction

The following results are published in the *International Journal of Nanomedicine and Nanosurgery*.[1]

Cancer is a leading cause of death in the US, with treatment being limited to non-selective methods, such as chemo, radio therapy, and surgery.[2] This has led to expansive interest in researching selective therapeutic methods to increase survival rates and general quality of life. The use of targeted nanoparticles (NPs) has been one approach.[2-4]

Hydrogel NPs have been shown to accomplish a variety of tasks in cancer treatment, such as imaging,[5] visible tissue delineation,[6] selective accumulation of chemo drugs,[7,8] photo-dynamic therapy (PDT),[9] photo-thermal therapy (PTT),[10] and sensing.[11] Each role is important either for probing the micro-environments of tumors to determine the most effective methods of treatment or enabling treatment. Specifically, PDT enjoys a vast quantity of interest due to its extreme selectivity and inherent lack of resistance from tumors.

PDT is the production of cytotoxic reactive oxygen species (ROS) when certain dyes (photosensitizers, PS) are excited under photo-illumination in the presence of oxygen. Therefore, PDT requires light, a PS, and oxygen to elicit cytotoxic effects. When combined in NPs that have been surface modified (peptides, antibodies, small molecules, etc.) to be cell-specific in uptake, extreme selectivity in treating cancer cells is achieved through selective accumulation.

Multiple photosensitizers capable of PDT have been employed (e.g. Photofrin, methylene blue, chlorin e6), but their relative aggressions in treating cancer using NPs are not well

characterized. Chlorin e6 (Ce6) has been used for therapy of both cancer and heart disease.[11-16] Here, we study the relative efficacy of Ce6 and methylene blue (MB) *in vitro,* when embedded in hydrogel polyacrylamide (PAAm) NPs, to evaluate their relative aggression in treating cancer. Previously reported MB-NPs are used for comparison.[17]

2.2 Results

2.2.1 Covalent Encapsulation of Ce6: Ce6 contains three aliphatic carboxylate groups that make it possible for the covalent attachment of the dye to our NPs. Covalent anchoring to the NP matrix is accomplished through the typical EDC/NHS reaction to primary amine containing monomers, which is then subsequently polymerized with the remaining monomers to form the hydrogel NPs. UV/VIS of the purified particles is presented in Figure 2-1; the canonical peak at 663nm is present.

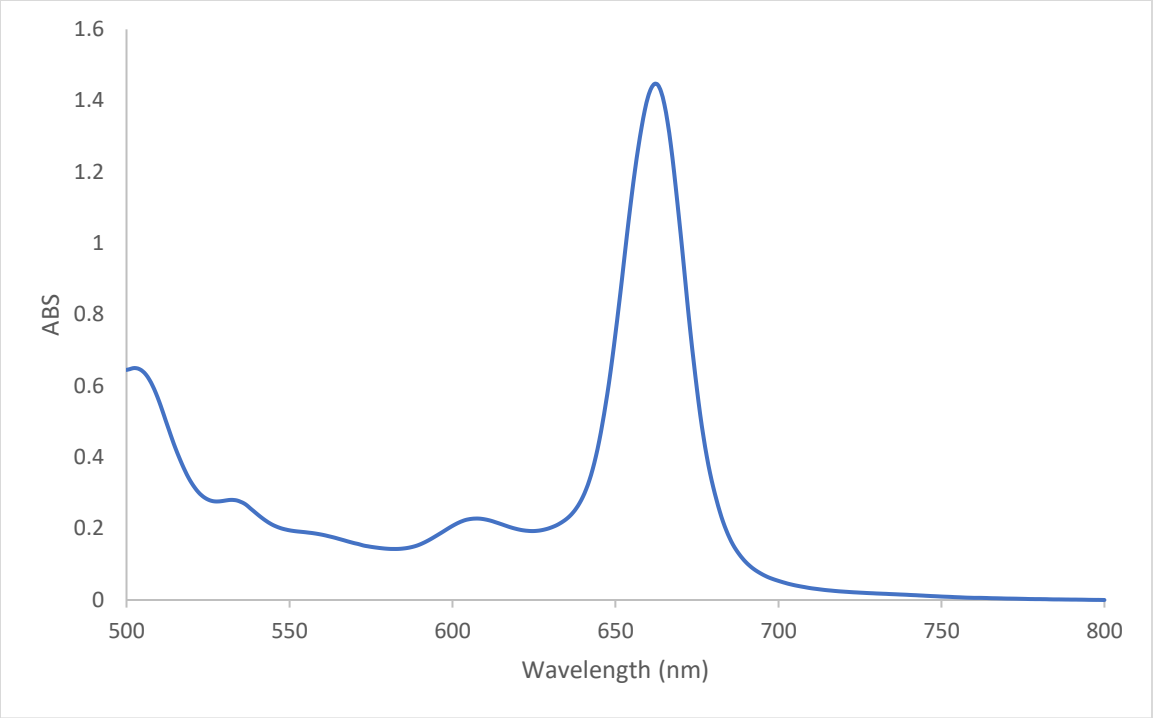

Figure 2-1: UV/VIS spectra of as prepared PAAm-Ce6 NPs at 1mg/mL in PBS. The soret band at ~400nm that is typical to porphyrins is omitted due to saturation of the detector.

In addition to the UV/VIS spectra, excitation and emission spectra are taken to show that that photo-physical properties are left unaffected (Figure 2-2). Fluorescence spectra was taken using the 663nm peak. However, because of the characteristic small stokes shift of porphyrin-based dyes (~1-2nm), the fluorescence peak is marginally clipped to avoid the detector picking up part of the excitation signal. It can be seen in Figure 2-2 that the Ce6 is still fluorescent and that the excitation spectra reflects the absorption spectrum of Figure 2-1.

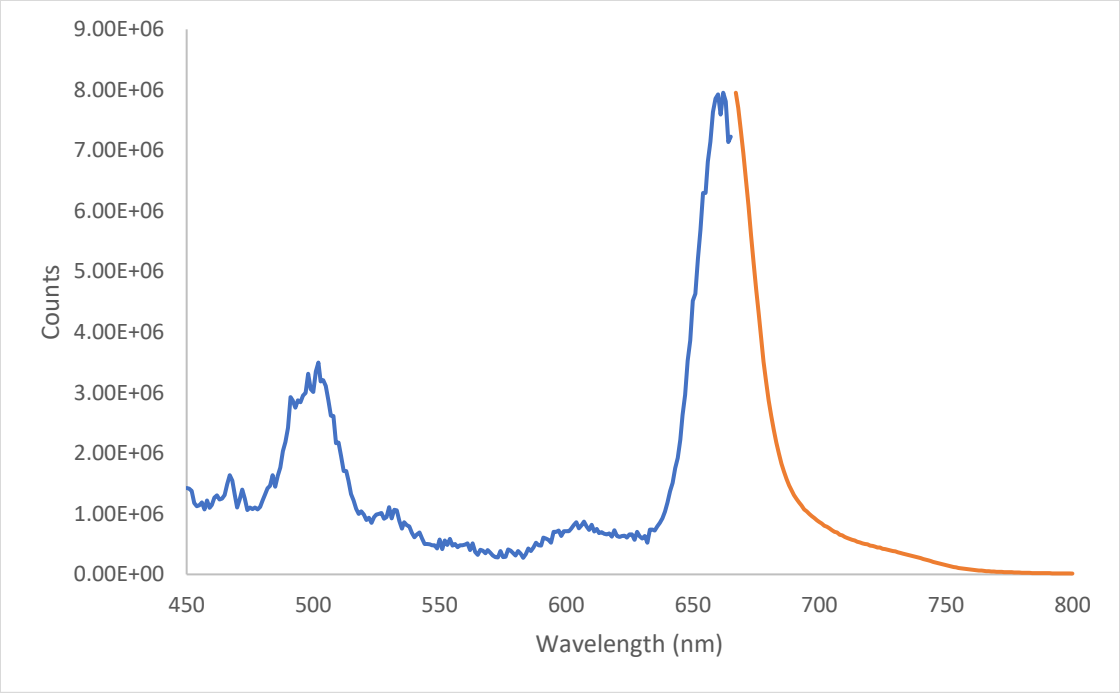

Figure 2-2: Ex/Em spectra of the as prepared PAAm-Ce6 NPs. The particles were dispersed in PBS at a concentration of 0.1mg/mL to avoid detector saturation. Excitation = Blue, Emission = Orange (663nm Ex).

In addition to the photo-physical properties of PAAm-Ce6, the general size of the NPs must be characterized to aid in evaluation of any toxicity data. Typically, dynamic light scattering (DLS) is employed as a method of characterizing hydrogel NPs, but the light source of these instrument is ~658nm. Due to this, characterization of PAAm-Ce6 NPs via DLS is not possible with the dye present. As an analogue method of analysis, NPs without Ce6 were synthesized. The size is found to be ~73nm (Figure 2-3).

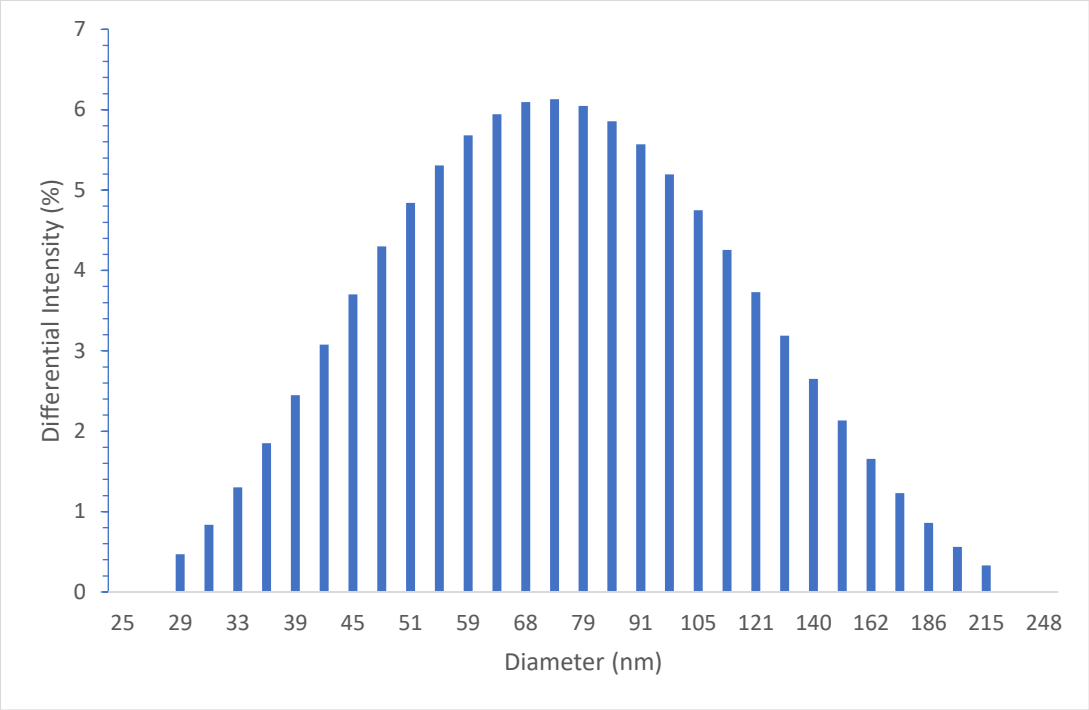

Figure 2-3: DLS of hydrated blank PAAm NPs. Mean diameter = 73nm, PDI = 0.204.

Transmission electron microscope (TEM) images of the PAAm-Ce6 NPs were also taken to provide a more direct understanding of the NP size (Figure 2-4). The size of these NPs is found to be ~17nm when dehydrated, similar in size to previously reported MB-NP TEMs (~14nm).

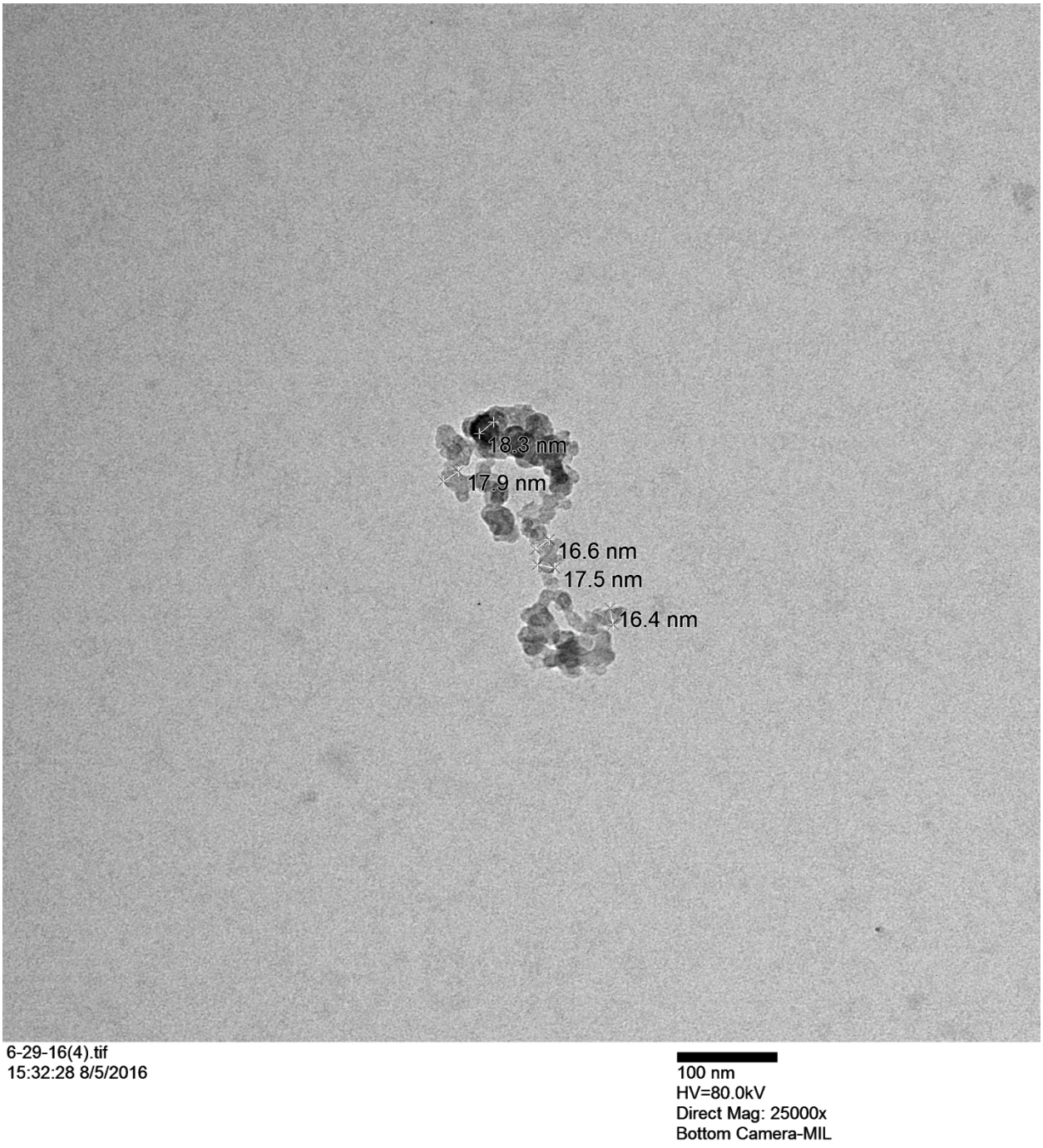

Figure 2-4: TEM images of dehydrated PAAm-Ce6 NPs. NPs were vacuum deposited onto the grid due to low adherence properties of hydrogel polymers on TEM grids.

2.2.2 ROS Generation in Solution: It is important to evaluate that Ce6 is still producing singlet oxygen. Although the preserved absorption and fluorescence properties indicate a preservation of ROS producing capabilities, it is important to note that Ce6 is still specifically producing type II ROS (singlet oxygen) and has not changed to predominantly producing type I (all other known species). To accomplish this, singlet oxygen sensing green (SOSG) is employed; SOSG specifically evaluates the presence of singlet oxygen and is insensitive to all other forms of ROS. Figure 2-5 shows a clear fluorescence enhancement of SOSG after illumination at 663nm in the presence of PAAm-Ce6 NPs.

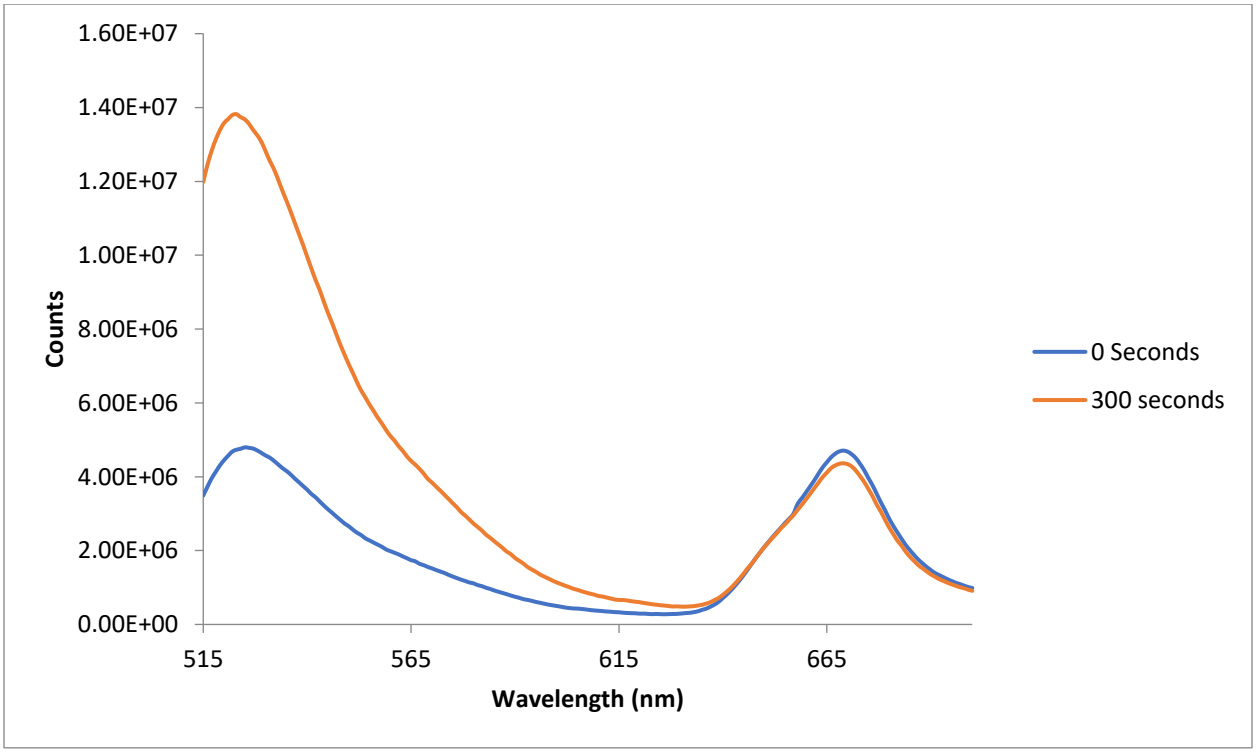

Figure 2-5: SOSG fluorescence before (0 seconds) and after a period of 663nm illumination (300 seconds) in the presence of PAAm-Ce6 NPs. The peak at ~665nm comes from Ce6.

2.2.3 In vitro PDT Efficacy: Before PDT testing of the PAAm-Ce6 NPs can be initiated, it is important to first test if there is any toxicity from the NPs alone with no illumination. To this end, HeLa cells are incubated with PAAm-Ce6 NPs overnight and evaluated using MTT assay. The results are shown in Figure 2-6; no significant toxicity is observed.

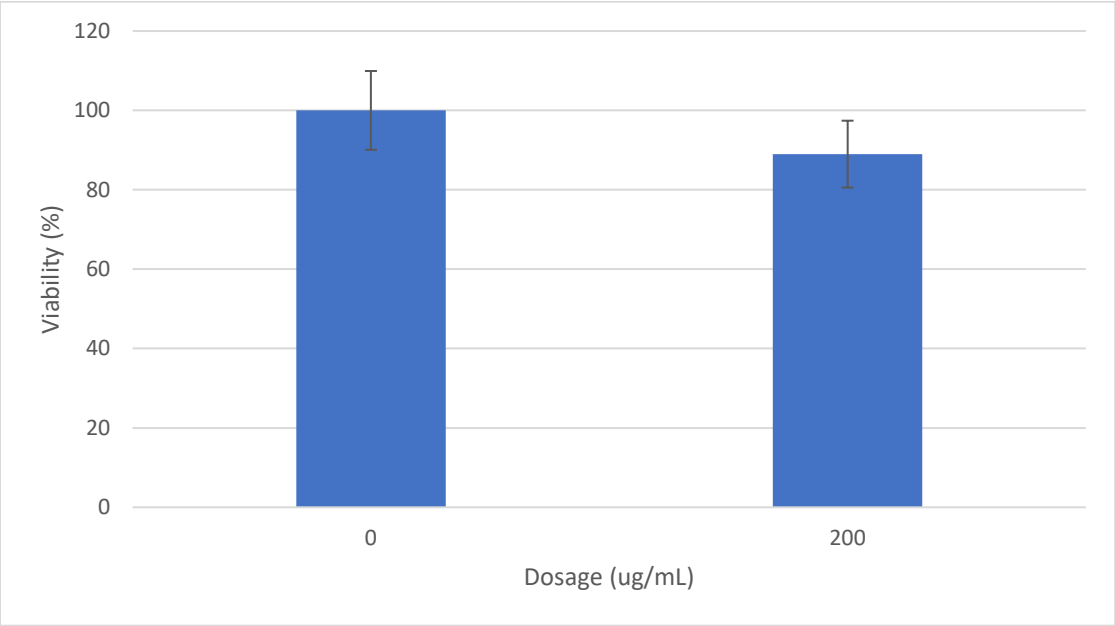

Figure 2-6: Dark toxicity of HeLa cells incubated with PAAm-Ce6 NPs overnight. Cells exposed to 200ug/mL were 89% viable.

Following establishing biocompatibility of the PAAm-Ce6 NPs their PDT efficacy was evaluated on a 96-well plate of HeLa cells with an LED array (625 +/- 20nm, 35.2mW). Using a dosage of 200ug/mL and 6min illumination, ~42% of the cells are killed (58% viable, Figure 2-7).

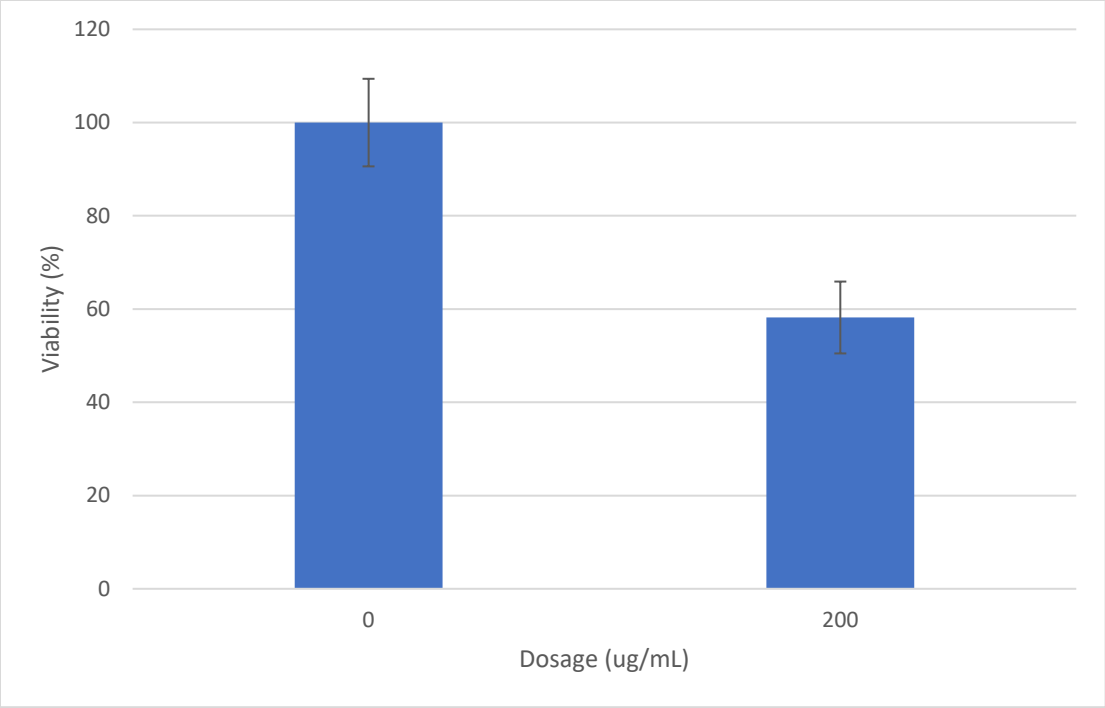

Figure 2-7: HeLa cell viability after PDT (6min, 625 +/- 20nm, 35.2mW). Cells incubated at 200ug/mL are ~58% viable post treatment.

Further analysis of PAAm-Ce6 NPs in PDT is done in comparison to previously reported MB-NPs. The relevant properties for discussion are shown in Table 1.

NPs	Wt% Loading	nmol dye/mg NP Loading	TEM (nm)	NP OD @ ~625nm	6min PDT Viability
Ce6	1.40	23.4	17	0.2	58%
MB	0.63	13.1	14	0.5	70%

Table 2-1: Comparative Data of Ce6 and MB-NPs.[17] OD = Optical Density at peak wavelength of light source, NP concentration = 1mg/mL. Note: Same light source and configuration used for both photosensitizers.

2.3 Discussion

A main feature of free Ce6 in aqueous and saline solutions is its tendency to aggregate. NPs generally act as an efficient means of reducing or eliminating aggregation by forcefully separating dye molecules from each other. Figures 2-1 and 2-2 show no signs of Ce6 aggregation via preservation of its 663nm peak and fluorescence. This is further reinforced by SOSG showing continued singlet oxygen production (Figure 2-5).

NPs may often be a source of toxicity in cells. This is typical in one of two ways: being overly positively charged (e.g. PAMAM dendrimer) or being too large. To evaluate the size of the NPs, DLS and TEM were employed. DLS of blank NPs (no dye, Figure 2-3) were ~73nm and TEM showed a size of ~17nm (Figure 2-4), similar to the as compared MB-NPs.[17] Therefore, the size of the PAAm-Ce6 NPs is within a biocompatible range. Dark toxicity of the PAAm-Ce6 NPs (Figure 2-6) confirms this by the low toxicity at a high concentration of 200ug/mL.

PDT of HeLa cells with PAAm-Ce6 NPs yielded a cell kill of 42% (Figure 2-7). This is remarkable when compared to previously reported MB-NPs under the same illumination conditions that aimed to optimize the production of ROS; the MB-NPs yielded a cell kill of 30%.[17] A difference of 30% vs. 42% may seem insignificant, but the meaning becomes more pronounced when the relative absorption spectra of the NPs is factored in. The PAAm-Ce6 NPs have an OD of 0.2 vs 0.5 for the MB-NPs at identical concentrations of 1mg/mL; the MB-NPs were less efficient at ablating cancer cells than the PAAm-Ce6 NPs while being ~2.5 times more absorbant in the range of active illumination. This overwhelmingly indicates that Ce6 is a more efficient dye for PDT than MB in NP-based systems.

It is also worth noting the shortcomings of the as presented system. The primary issue faced with the NPs is the diminished hydrophilicity with increasing Ce6 loading. This is not entirely unexpected, as the hydrophilic groups of the dye are co-opted for covalent attachment. In this aspect, MB is a more desirable dye due to its exceptionally higher aqueous solubility. The lowered solubility of the PAAm-Ce6 NPs would also decrease their overall efficacy *in vivo*, where high administration dosages of 20-50mg/mL are necessary. Optimization of dye loading, matrix design, and synthetic conditions will likely yield NPs with greater hydrophilicity and thus animal model viability.

2.4 Conclusions

The PS Ce6 was successfully encapsulated in a PAAm hydrogel through standard EDC/NHS coupling reaction while preserving its basic photo-physical properties. The as prepared PAAm-Ce6 NPs displayed low toxicity in the dark at a high concentration of 200ug/mL and greater *in vitro* PDT capacity than previously reported MB-NPs. It is therefore understood that the PS Ce6 is a superior candidate in NP-PDT when compared the classical golden standard PS MB.

2.5 Acknowledgements

We would like to acknowledge the Microscopy and Image Analysis Laboratory of the University of Michigan for gather the TEMs.

2.6 Materials and Methods

Materials: All materials were sourced from Sigma Aldrich. acrylamide (AAm), amino propyl methylacrylamide (APMA), 3-(acryloyloxy)-2-hydroxypropyl-methacrylate (AHM), dioctyl sulfosuccinate sodium salt (AOT), Brij 30, 1-Ethyl-3-(3-dimethylaminopropyl) carbodiimide (EDC), N-hydroxy succinidmide (NHS), dimethyl sulfoxide (DMSO), phosphate buffer saline (PBS, 0.01M), ammonium persulfate (APS), tetra methyl ethylene diamine (TEMED), phosphate buffer saline (PBS).

Preparation of PAAm-Ce6 NPs: 1.07g of AOT, 2.2mL Brij 30, and 30mL Hexane are combined in a 100mL round bottom flask. An aqueous phase of 28mg APMA, 368mg AAm, 52.6uL AHM, 40mg EDC, 60mg NHS, 100uL DMSO, and 930uL PBS are prepared and added to the round bottom flask. The contents of the flask are stirred for 2 hours at 500 RPM. The contents are then flushed with argon using a long neck needle in contact with the mixture for 15 minutes. Argon flow is then continued but removed from contact with the mixture. 15mg of APS in 100uL of water is added drop wise to the flask to initiate polymerization. 100uL of TEMED is added drop wise and the reaction allowed to continue for 2 hours under argon. Argon is then removed, and the contents of the flask exposed to oxygen to quench polymerization. Hexane is rotary evaporated, and the leftover contents are cleaned in an amicon cell (300kDa membrane) with 10x150mL ethanol and 5x150mL Millipore water. The final product dispersed in Millipore water is filtered using a 0.45um polyether sulfonate filter and lyophilized to obtain a solid product. Samples are stored in a freezer until needed.

Singlet Oxygen Test: ROS production was tested using Singlet Oxygen Sensing Green (SOSG). A 1mg/mL sample (2mL, PBS) was given 10uL of 0.5mM SOSG in methanol and

illuminated at 663nm for 5min. The fluorescence of SOSG was measured at 504/525nm Ex/Em before and after illumination.

Size analysis: TEMs were taken through the Microscopy and Image Analysis Laboratory at the University of Michigan. Samples were deposited on grids via vacuum evaporation of solvents and subsequent staining with uranyl acetate. Blanks of NPs (no dye) were synthesized and characterized using dynamic light scattering (DLS, Delsa Nano C Particle Analyzer).

Photo-Physical Properties: Absorption spectra were gathered using a Shimadzu UV-1601 UV-Visible Spectrophotometer and all fluorescence-based work done using a Fluoromax 3.

Cell Culture: 96-well plates were seeded with 2000 HeLa cells per well (n = 16) containing 200uL of media. Plates of light and dark toxicity were given NP dosages of 0 and 200ug/mL; 0 ug/mL were control groups that defined 100% viability. Cell viability was determined colorimetrically in a plate reader via MTT assay. Briefly, cell media was replaced with colorless media containing no serum (100uL) and 20uL of 5mg/mL MTT reagent and incubated for 4 hours. The media was then carefully removed and the formazan crystals solubilized using 100uL of DMSO. Light toxicity was investigated by illuminating the 96-well plate using an LED array (625nm +/- 20nm, 35.2mW) for 6min.

2.7 References

[1]Hopkins, T.; Ukani, R.; Kopelman, R. Intracellular Photodynamic Activity of Chlorin e6 Containing Nanoparticles. *Int. J. Nanomed. Nansurg.*, 2016, **2**, 119. DOI: 10.16966/2470-3206.

[2]Gupta et al. Polyacrylamide-Based Biocompatible Nanoplatform Enhances the Tumor Uptake, PET/fluorescence Imaging and Anticancer Activity of a Chlorophyll Analog. *Theranostics*, 2014, **4**, 614 – 28. DOI: 10.7150/thno.8478.

[3]Xin, Y.; Huang, Q.; Tang, J.Q.; Hou, X.Y.; Zhang, P.; Zhang, L.Z.; Jiang, G. Nanoscale drug delivery for targeted chemotherapy. *Cancer Lett.*, 2016, **379**, 24 – 31. DOI: 10.1016/j.canlet.2016.05.023.

[4]"Targeted, Multifuncional Hydrogel Nanoparticles for Imaging and Treatment of Cancer" R. Kopelman and Y.E.K. Lee, Chapter in "*Multifunctional Nanoparticles for Drug Delivery Applications*", Springer, Editor: Sonke Svenson, ch. 11, p.225-255 (2012).

[5]Natarajan, A.; Xiong, C.Y.; Gruettner, C.; DeNardo, G.L.; DeNardo, S.J. Development of Multivalent Radioimmunonanoparticles for Cancer Imaging and Therapy. *Cancer Biother Radiopharm.*, 2008, **23**, 82 – 91. DOI: 10.1089/cbr.2007.0410.

[6]Nie et al. Hydrogel Nanoparticles with Covalently Linked Coomassie Blue for Brain Tumor Delineation Visible to the Surgeon. *Small*, 2012, **8**, 884 – 91. DOI: 10.1002/smll.201101607.

[7]Surnar, B.; Sharma, K.; Jayakannan, M. Core-shell polymer nanoparticles for prevention of GSH drug detoxification and cisplatin delivery to breast cancer cells. *Nanoscale*, 2015, **7**, 17964 – 79. DOI: 10.1039/c5nr04963f.

[8]Shirakura, T.; Kelson, T.J.; Ray, A.; Malyarenko, A.E.; Kopelman, R. Hydrogel Nanoparticles with Thermally-controlled Drug Release. *ACS Macro. Lett.*, 2014, **3**, 602 – 6. DOI: 10.1021/mz500231e.

[9]Tang, W.; Xu, H.; Park, E.J.; Philbert, M.A.; Kopelman, R. Encapsulation of Methylene Blue in Polyacrylamide Nanoparticle Platforms Protects its Photodynamic Effectiveness. *Biochem. Biophys. Res. Commun*,, 2008, **369**, 579 – 83. DOI: 10.1016/j.bbrc.2008.02.066.

[10]Curry, T.; Epstein, T.; Smith, R.; Kopelman, R. Photothermal therapy of cancer cells mediated by blue hydrogel nanoparticles. *Nanomedicine*, 2013, **8**, 1577 – 86. DOI: 10.2217/nnm.12.190.

[11]Hathaway et al. Detection of breast cancer cells using targeted magnetic nanoparticles and ultra-sensitive magnetic field sensors. *Breast Cancer Res.*, 2011, **13**, R108. DOI: 10.1186/bcr3050.

[12]Varchi, G. et al. Chlorin e6 keratin nanoparticles for photodynamic anticancer therapy. *RSC Adv.*, 2016, **6**, 33910 – 8. DOI: 10.1039/c6ra04208b.

[13]Shton, I.O.; Sarnatskaya, V.V.; Prokopenko, I.V.; Gamaleia, N.F. Chlorin e6 combined with albumin nanoparticles as potential composite photosensitizer for photodynamic therapy of tumors. *Exp Oncol.*, 2015, **4**, 250. DOI:

[14]Zhang, D.; Wu, M.; Zeng, Y.; Wu, L.; Wang, Q.; Han, X.; Liu, X.; Liu, J. Chlorin e6 Conjugated Poly(dopamine) Nanospheres as PDT/PTT Dual-Modal Therapeutic Agents for Enhanced Cancer Therapy. *ACS Appl. Mater. Interfaces.*, 2015, **7**, 8176 – 87. DOI: 10.1021/acsami.5b01027.

[15]Avula, U.; Yoon, H.; Kim, G.; Kopelman, R.; Kalifa, J. Left Atrium Nanoplatform-enabled Targeted Photodynamic Ablation: Preliminary Results in Vivo. *Heart Rhythm*, 2013, **10**, 1747. DOI: 10.1016/hrthm.2013.09.033.

[16]Avula et al. Cell-selective arrhythmia ablation for photomodulation of heart rhythm. *Sci. Transl. Med.*, 2015, **7**, 311ra172. DOI: 10.1126/scitranslmed.aab3665.

[17]Yoon, H.K.; Lou, X.; Chen, Y.; Lee, Y.K.; Yoon, E.; Kopelman, R. Nano-photosensitizers Engineered to Generate a Tunable Mix of Reactive Oxygen Species, for Optimizing

Photodynamic Therapy, Using a Microfluidic Device. *Chem. Mater.*, 2014, **26**, 1592–1600. DOI: 10.1021/cm403505s.

Chapter 3: An Ultra-Compact Nano-Theranostic PEG Platform for Cancer and Heart Arrhythmia

3.1 Introduction

The following is currently in submission to *ACS Applied Bio Materials*.[1]

We describe here a multi-functional, ultra-small, nanoplatform that has a plethora of desirable therapeutic and diagnostic (theranostic) properties. Specifically, we demonstrate its superior photodynamic efficacy, illustrated by its application to cancer cells. We also emphasize its unique performance as an excellent, non-toxic, molecular imaging agent for MRI.

Photodynamic therapy (PDT) is a method for ablating biological tissue by photo-oxidation utilizing photosensitizer (PS) molecules. PDT has been pioneered by Dougherty and co. at the Roswell Park Cancer Institute for treatment of skin cancer and other diseases.[2,3] Since the start of the millennium, the field has received additional attention due to the emergence of *cell-targeted PDT*. Both spatial (laser focused) and biological (cell selective) selectivity is achieved by employing nanoconstructs (NCs) with targeting antibodies or peptides, which also extended PDT treatment to subsurface tumors.[3-9] In general, the use of NCs allows for protection of a PS from the bio-environment, and *vice versa*, for bypassing the immune system[4-13]

Recently, we reported on the use of PDT for treating *heart arrhythmia* in rat and sheep models.[14] The NC utilized was the octopus-like, ultra-compact and highly biocompatible polymer, *8-arm polyethylene glycol amine (*8PEGA*)*. The amine terminated arms were used to anchor the algae derived PS, chlorin e6 (Ce6), and a targeting moiety for cardio-myocytes.[14] Here, the relatively small sized (<20nm) 8PEGA derived NCs penetrated the very dense tissue of

the heart muscle, selectively accumulating in cardio-myocytes, and thus allowing their photodynamic ablation under mild near infrared illumination. Given the success of cell-selective heart arrhythmia ablation, we focus here on adapting an analogous NC for treating cancer.

In the heart arrhythmia project, the method of tagging 8PEGA with CTP (cardiac targeting peptide) for targeting was the very well understood maleimide-thiol reaction. Similarly, we expect any peptide to be viable for attachment 8PEGA, provided it is cysteine terminated. The F3-cys peptide is a specific cancer targeting peptide studied by our lab at great length.[9,15] It was thus chosen as our test case for extending the application of 8PEGA-Ce6 from arrhythmia to cancer. HeLa cells were chosen as the model system of interest due to their robust nature and known over-expression of nucleolin,[16] the specific target of the F3-cys peptide.[15] While our initial interest in 8PEGA stemmed from its small size, (sufficient to penetrate heart muscles) and its biocompatibility, in this work we focus on: 1) its ability to optimize ROS production with a given PS, and 2) its ability to function as a molecular imaging agent for MRI. The optimized ROS production is expected for this NC due to the direct contact of the PS Ce6 with the oxygenated environment, in contrast to when it is encapsulated inside a standard model matrix, such as in Polyacrylamide hydrogel nanoparticles (PAAm NPs).[17] We demonstrate here an increased ROS production efficacy, biocompatibility, and flexibility in targeting when utilizing this NC.

The high molecular weight (40 kDa), flexible chain dynamics of the 8PEGA group, and its specific structure, also create favorable conditions for highly selective molecular imaging using MRI. Specifically, the slow diffusion constant and transverse spin relaxation rate of 8PEGA combine to allow diffusion weighted MRI sequences which suppress surrounding water and fat signals, providing a very clean image of 8PEGA. We show here that the 8PEGA MR

signal is selectively detected and is proportional to its concentration. We also emphasize its biocompatibility, compared to current heavy metal atom MRI imaging agents.

3.2 Results

3.2.1 Complete 8PEGA Characterization: We compared the ROS production of Ce6 when attached to 8PEGA *vs.* when encapsulated in polyacrylamide (PAAm), where the two competing nanostructures are represented in Figure 3-1. Figure 3-2 contains the "*k-value*" plot of the relative ROS production of PAAm encapsulated Ce6. The *k*-value is a measure of the kinetic rate at which ROS is produced by Ce6, as measured by the first order decay of ADPA fluorescence. While the *k*-value of 8PEGA was determined by us before,[14] to generate *k*-values that are comparable, the OD of the PAAm-Ce6 NPs[17] was adjusted by UV/VIS to the Optical Density (OD, 0.12) of the previously reported 8PEGA-Ce6 at 660nm.[14] Table 3-1 shows the relative results for the two NCs when normalized for their literature ODs.

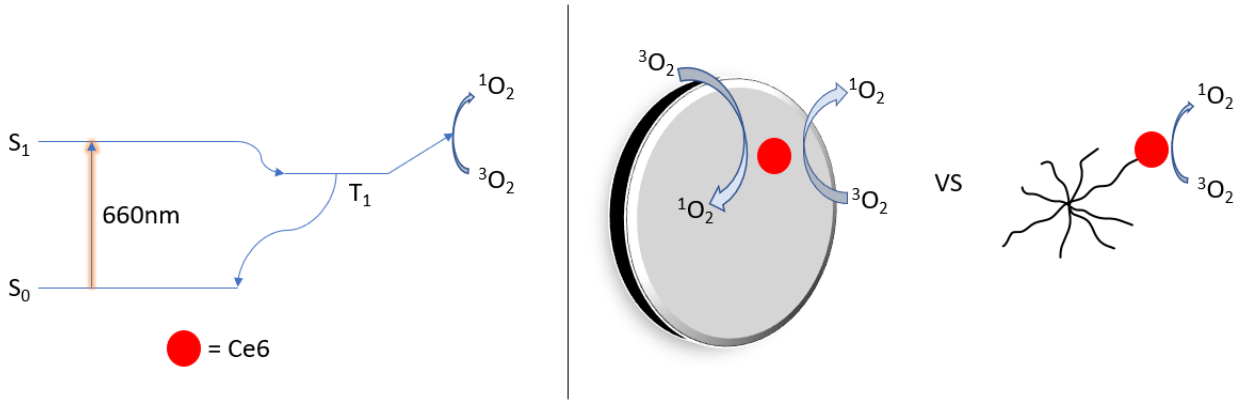

Figure 3-1: Difference in structural representation of Ce6 delivery and ROS production efficacy (not drawn to scale). Left: basic Jablonski diagram of how ROS is produced by Ce6. Right: Encapsulated Ce6 vs anchored to 8PEGA; difference in how ROS may move show a clear change in efficacy.

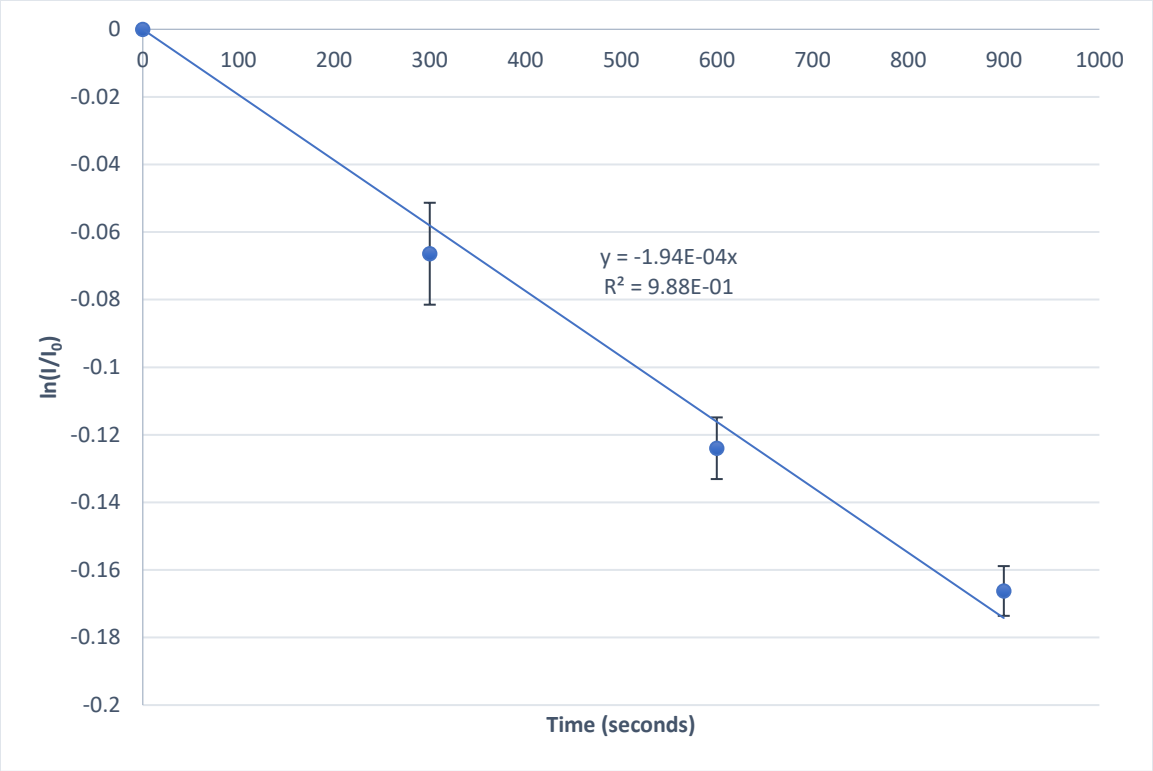

Figure 3-2: *k-value* plot of Ce6 encapsulated in PAAm NP as tracked by ADPA fluorescence quenching over time. The 660 nm OD = 0.12 in PBS; the slope of the plot is the *k-value*.

Nanoplatform	OD	*k-value*
8PEGA-Ce6	0.12	2.99E-04 s^{-1}
Ce6/PAAm NP	0.12	1.94E-04 s^{-1}

Table 3-2: *k-values* of the two discussed NCs at OD = 0.12 for 660nm.

Figure 3-3 is a wet transmission electron microscopy (TEM) of 8PEGA on a copper grid that has been negative stained with uranyl acetate. The size of the 13 measured NCs is found to be consistent with a ~10 – 12nm range, matching the Stokes-Einstein approximation (calculated in section 3.2.4) of the material.

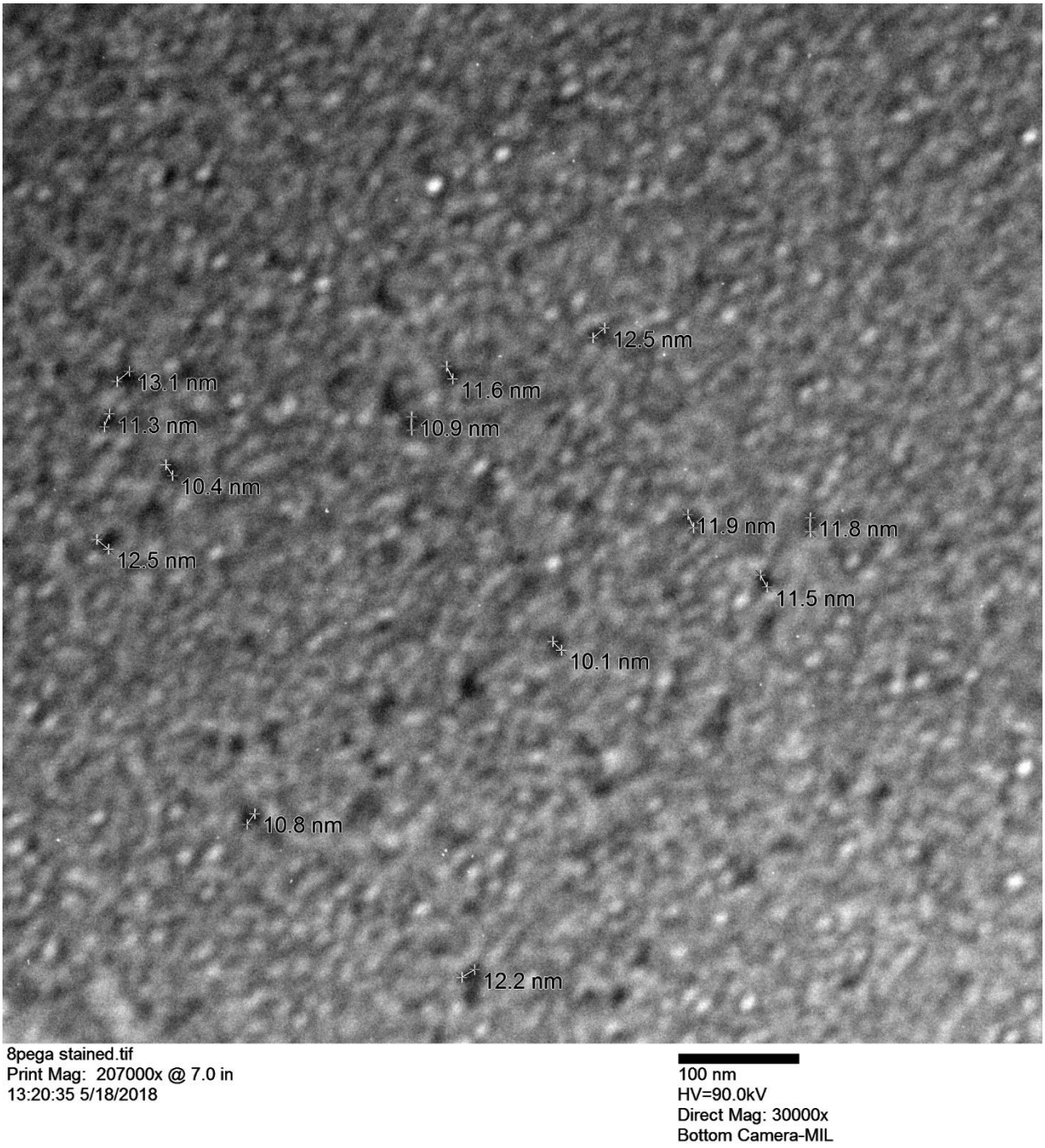

Figure 3-3: TEM of 8PEGA negatively stained with uranyl acetate.

Figure 3-4 shows the absorption spectrum of the F3-8PEGA-Ce6 conjugate; we find that the characteristic peaks at 660 nm are preserved, compared to the non-targeted NCs.[14] For clarity, the chemical modification of 8PEGA-Ce6 with F3-cys is shown in Scheme 3-1.

Scheme 3-1: Modification of 8PEGA-Ce6 with F3-cys peptide, as reported in this paper.

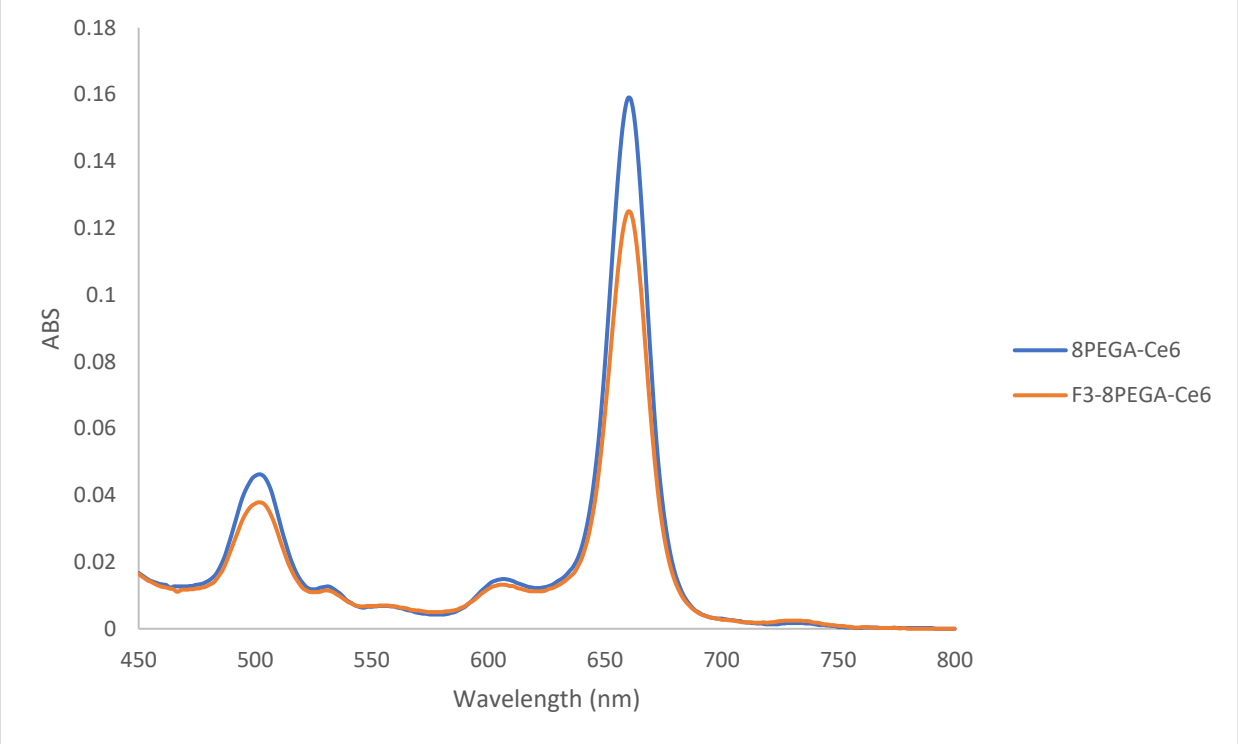

Figure 3-4: UV/VIS spectrum of 8PEGA-Ce6 and F3-8PEGA-Ce6 in PBS at 0.1 mg/mL.

3.2.2 Dark Toxicity of HeLa 229 cells: Flow cytometry was employed as a method of testing the biocompatibility of this NC to test for dark toxicity. Cells were tested at a concentration of

200ug/mL F3-8PEGA-Ce6; control cells denote a data group with no F3-8PEGA-Ce6 NCs added. As can be seen from Figure 3-5, no significant toxicity was observed.

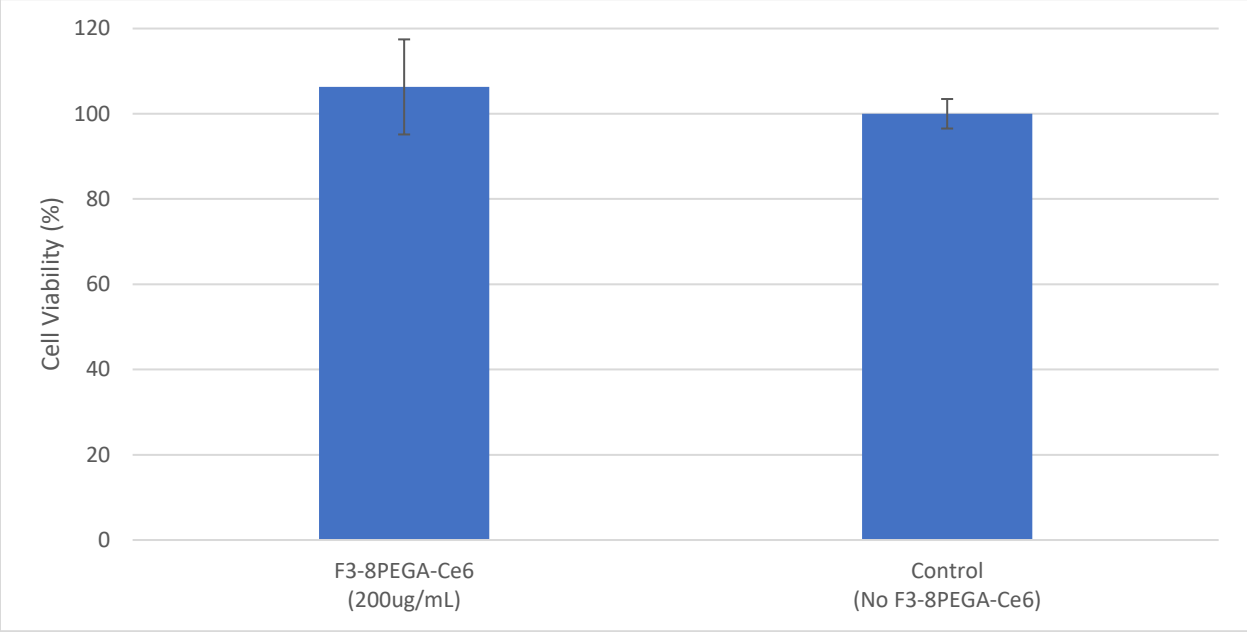

Figure 3-5: Hemocytometry Cell Population Results. Incubation conditions: 200 ug/mL F3-8PEGA-Ce6 for 24 hours in wells seeded with 200,000 cells; N = 3x3 for control and test groups (3 plates each, tested 3 times each). Control group of cells contain no F3-8PEGA-Ce6 NCs, under the same conditions. The results show near identical cell populations.

3.2.3 PDT Efficacy in vitro: As a control test to eliminate the possibility of simple cell stress from the excitation light, HeLa cells without F3-8PEGA-Ce6 were plated and illuminated for the same length of time and power as used in PDT for NC-treated cells (50mW/cm^2, 10min). After illumination (Figure 3-6A, B) there is an insignificant change in cell morphology, no change in the cytosolic stain calcein AM fluorescence counts, and no signs of membrane blebbing (a hallmark of apoptosis).

We observe a remarkable difference in the calcein AM fluorescence after photo-illumination of the cells with F3-8PEGA-Ce6 (Figure 3-6C, D). While there was no observable propidium iodidie (PI) fluorescence prior to illumination (data not shown), after illumination cell membrane impermeable PI can be seen to stain the nuclei of the cells (Figure 3-6E).

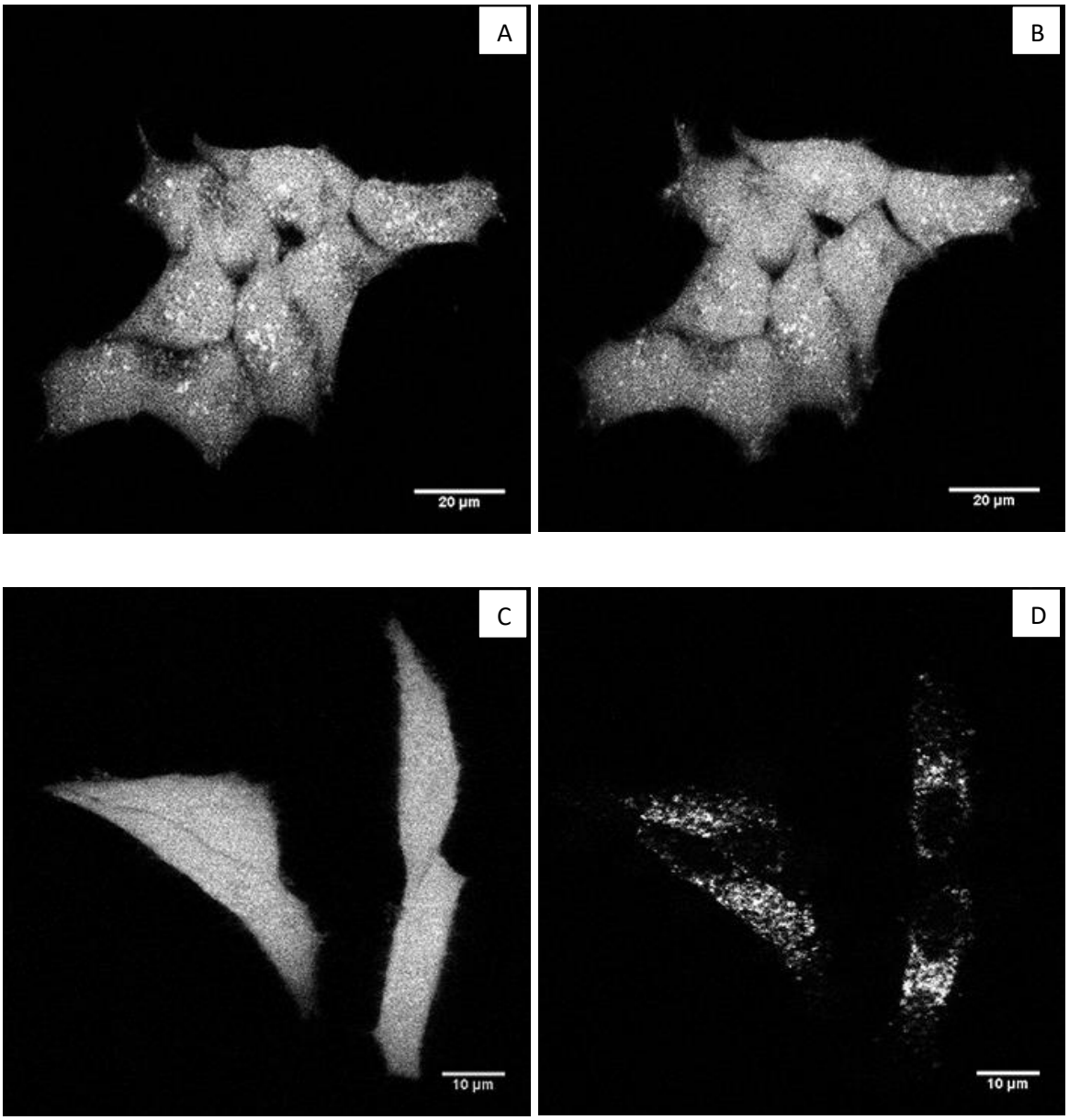

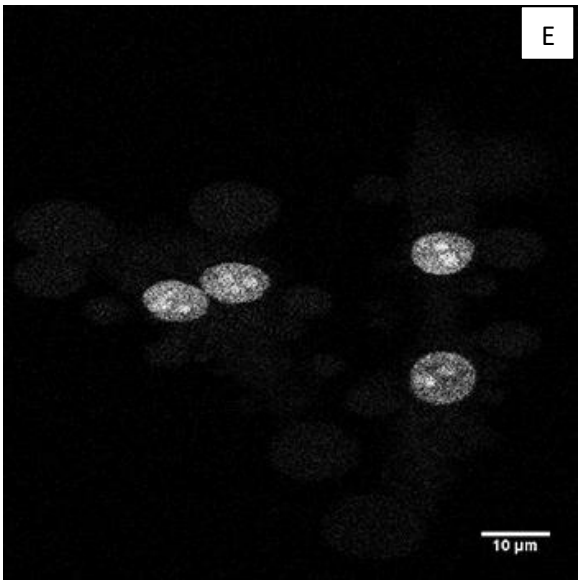

Figure 3-6: PDT testing images of HeLa 229 cells. A) Calcein AM fluorescence of PDT control cells (no F3-8PEGA-Ce6). B) Calcein AM fluorescence of PDT control cells 2 hours after illumination. C) Calcein AM fluorescence of test cells (with F3-8PEGA-Ce6) prior to PDT. D) Calcein AM fluorescence of test cells 2 hours after PDT. E) PI fluorescence 2 hours after PDT. PDT test plates were incubated with 200ug/mL F3-8PEGA-Ce6 for 2 hours prior to PDT and all cells illuminated at a total fluence of 50mW/cm^2 for 10 minutes, using a 692 +/- 20nm filter and arc lamp.

3.2.4 MRI/NMR Characterization of 8PEGA: The translational diffusion constant, D, and relaxation times T_1 and T_2 of 8PEGA were measured at 25 and 35 °C (Table 3-2). Images in solution of 8PEGA (non-modified) were gathered to demonstrate generation of clean images when water/fat suppressed (Figure 3-7) and their concentration dependent response (Figure 3-8). The response can be seen to be linear with concentration (Figure 3-8), consistent with images

gathered with water suppression techniques (Figure 3-7B). Tested concentrations were 0, 2.38, 4.77, 9.54, and 19.08 mg/mL 8PEGA in H_2O. In addition, the Stokes-Einstein equation:

$$r = kT/6\pi\eta D_{\text{trans}}$$

is employed to calculate the size of 8PEGA to verify TEM results; the diameter is calculated to be 10.96nm at 35 °C.

T (°C)	T_1 (ms)	T_2 (ms)	D (10^{-11} m^2/s)
25	791 ± 36	586 ± 24	3.572 ± 0.015
35	934 ± 72	769 ± 31	4.923 ± 0.018

Table 3-2: Relaxation times and translational diffusion constant of 8PEGA at 25 and 35 °C measured at 16.4 T. Sample is 5mg/mL 8PEGA in 25/75 (V/V) H_2O/D_2O.

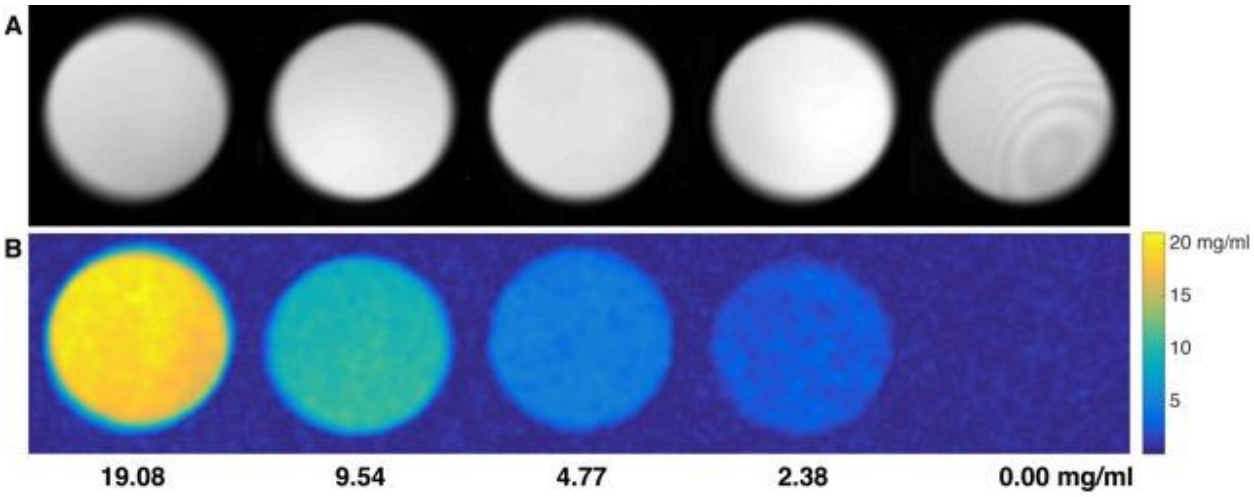

Figure 3-7: Diffusion-weighted spin-echo MR images of 8PEGA obtained with b = 10^8 s/m^2 (A) and b = 10^{10} s/m^2 (B). The 110 M water proton signal dominates conventional MR images as seen in (A) but is suppressed by a factor of 10^{-10} by imaging at b = 10^{10} s/m^2. The diffusion constant of 8PEGA was measured by stimulated echo pulsed field gradient NMR at 25 °C to be

3.572 10^{-11} m^2/s, allowing 70% of the initial magnetization to survive at b = 10^{10} s/m^2. The color bar in the (B) shows detected concentration of 8PEGA.

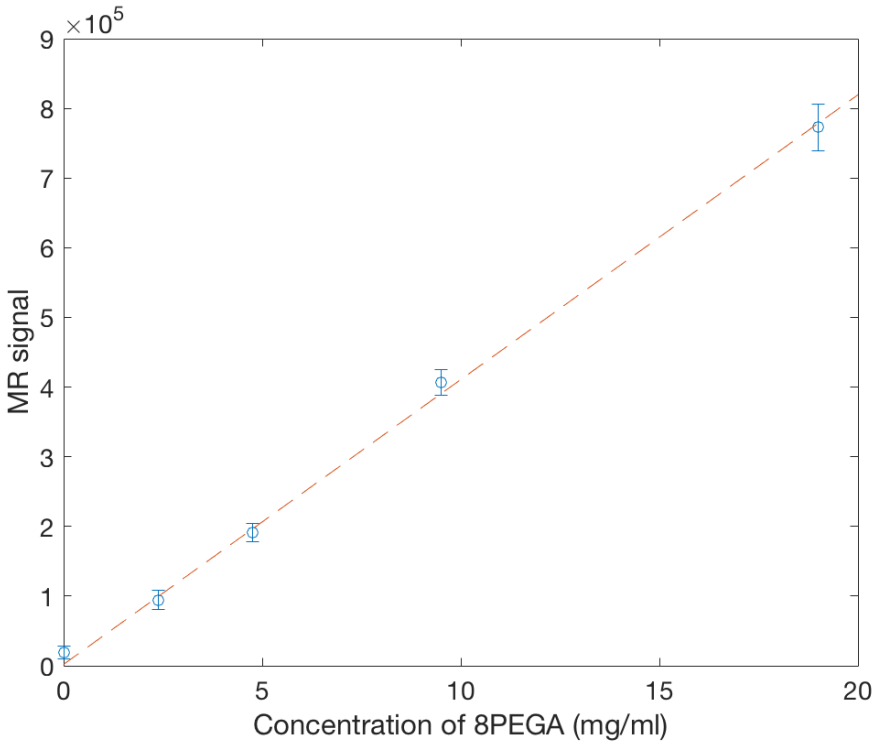

Figure 3-8: Concentration dependent MRI signal of 8PEGA. A region of interest (ROI) was selected for each of the 5 vials and mean (circles) and standard deviation (error bars) of the signal computed. A linear equation was fitted to the 5 measured vials and the result is shown as a dashed line.

3.3 Discussion

We hypothesized that Ce6-8PEGA would be a more efficient ROS producing platform, compared to hydrogel NPs, based on the understanding that in 8PEGA the Ce6 group is in direct contact with the oxygenated environment of the cells (Figure 3-1). Thus, oxygen does not need to diffuse into a PAAm NP matrix encapsulating the PS and the ROS need not diffuse out, nor

suffer losses due to reaction with the matrix. The *k-value* test confirms this hypothesis by showing that, when adjusted to identical ODs, the *k-value* of the Ce6-8PEGA[14] is about 50% larger than that of the Ce6 encapsulated PAAm NPs (Table 3-1).

Being that 8PEGA is a star shaped polymer, measurement of its size by the Stokes-Einstein Equation, which assumes a spherical material shape, is desirable.[18] It is found after measuring the translational diffusion coefficient, D (Table 3-2), that the size of polymer at 35 celcius is ~11nm. As a secondary method of analysis, 8PEGA stained with uranyl acetate and visualized using TEM (Figure 3-3). The size of the 13 chosen points is found to be approx. 10 – 12nm, in good agreement with the Stokes-Einstein Equation measurement.

PEGylating the surface of nanoparticles is often used as a sort of cloak and dagger approach, as PEG is largely ignored by the immune system and cells in general.[19] Here the platform itself is made of PEG only. Thus, a targeting vector is helpful not only for *in vivo* applications but even to accelerate cell uptake *in vitro*. For cancer targeting, the nucleolin targeted peptide F3-cys has been shown to be quite useful and was thus chosen for grafting onto the 8PEGA-Ce6.[20-23] Notably, after attachment of F3-cys, the Ce6 spectroscopic features are largely unaffected (Figure 3-4), indicating the preservation of photophysical properties when switching peptides (from CTP for targeting heart myocytes to F3 for targeting cancer cells).[14-16] A mild decrease in Ce6 absorption is noted for 0.1mg/mL when compared to before and after modification, but is expected, as the BiPEG and F3-cys will increase the MW of the NC.

An important aspect of this NC is its biocompatibility. The total construction is comprised of PEG, Ce6, and the homing peptide F3-cys. PEG is commonly known as a highly biocompatible substance and F3-cys has been used as a targeting agent in our lab and others with no toxic effects *in vitro* or *in vivo*.[20-23] The algae derived Ce6 has been used extensively in the

literature as a PDT agent.[24-28] As such, it is expected that the combination of these three moieties should present no significant biocompatibility issues. This is confirmed *in vitro* by our hemocytometry results (Figure 3-5).

Before initiating PDT tests with F3-8PEGA-Ce6, the chosen laser conditions (50mW/cm^2 for 10min) were tested to ensure that the illumination was not a source of significant cell stress. Calcein AM images of the cells before (Figure 3-6A) and after (Figure 3-6B) illumination demonstrated little change in morphology and no signs of apoptosis. Therefore, the photo-illumination source does not impart significant stress upon the cells. PDT was then initiated in the presence of F3-8PEGA-Ce6 at a concentration of 200ug/mL (Figures 3-6C/D/E). There is a significant decrease of calcein AM fluorescence after PDT, indicating a loss of cytosolic contents, an event that would only occur under conditions where the cell membrane has been ruptured. Rupturing of the membrane was shown by the staining of the nuclei with the cell impermeable dye PI (Figure 3-6E). Taking the PDT test results in conjunction with the cyto-compatibility in Figure 3-5, it is evident that the death of the cells is PDT-mediated.

In addition to the more efficient PDT (50% larger *k*-value), we believe that the use of 8PEGA NPs may present two more advantages: (1) The small size of the NC offers the possibility of quick renal clearance from the body,[14] a feature not afforded by larger NPs, and (2) the ability to penetrate tumor areas that have not yet undergone angiogenesis, in contrast to traditional larger NPs that require a porous/leaky vasculature so as to be able to penetrate the tumor.[29]

Previous work has shown that ^{13}C tagged PEG could be selectively imaged *in* vivo using heteronuclear MR methods.[30] We report here that the intrinsic flexibility of the polyethylene oxide chain[31] and the slow translational diffusion of 8PEGA create an exploitable set of physical

and dynamic conditions for selective MR imaging of 8PEGA protons using ^{1}HNMR. Specifically, 8PEGA's fast chain motions with correlation times of approximately 0.1ns[31] provide sufficient averaging of the proton dipole-dipole interaction to yield a long nuclear spin transverse relaxation time T_2, measured here to be 586 and 769ms at 25 and 35 °C, respectively. In contrast to fast internal chain dynamics, the molecule's high molecular weight yields a translational diffusion constant that is two orders of magnitude slower than that of water molecules. Therefore, the water signal can be effectively suppressed by large diffusion gradients[32] so that only the ethylene oxide signal will remain due to the combination of its long T_2 time and slow diffusion if 8PEGA. Notably, the MR signal intensity decays as:

$$M_{xy}(b, TE) = M_{xy}(0)e^{-bD}e^{-TE/T_2}$$

where the *b value* is determined by the magnetic field gradient magnitude and duration, *D* is the translational diffusion constant of either water or 8PEGA, TE is the echo time, and T_2 is the transverse spin relaxation time. In addition, the symmetry of the ethylene oxide monomer gives rise to a single chemical shift for all four protons and each 40kDa polymer molecule caries approximately 3,600 protons, creating a large molar amplification of the NMR or MRI signal. By performing a diffusion-weighted, spin-echo MR imaging experiment with high *b* values and long TE times, water signals, due to fast diffusion, and fat signals, due to short T_2 times, are effectively suppressed and the *8PEGA* signal selectively imaged. *In vivo*, some signal at high *b* values will remain due to restricted diffusion in cells, but these signals can either be removed or distinguished from the 8PEGA signal due to the ~1 ppm difference between water and ethylene glycol protons in traditional ^{1}HNMR.

The results (Figure 3-7A, B) indeed show that 8PEGA functions very well as an MR imaging agent when coupled with the above-mentioned suppression techniques. This may

potentially replace other MRI contrast agents like gadolinium salts or chelates, which present health risks to certain patient groups. There is a clear difference in images without (Figure 3-7A) and with (Figure 3-7B) applied suppression techniques. The 8PEGA imaging signal is also linear with its concentration (Figure 3-8). Notably, when the above techniques are applied, clean and well-defined images of 8PEGA are recovered, showing clearly its viability as a potential imaging agent *in vivo*. If properly calibrated for, this would allow for quantification of the 8PEGA in biological tissue (e.g. tumor area vs filtration organs).

3.4 Conclusion

The Ce6-8PEGA NCs have been shown to be ultra-small and possess superior ROS production, compared to encapsulated PAAm-Ce6 NPs. The successful exchange of the targeting peptides, from CTP to F3-cys, demonstrates this NC's chemical flexibility in changing targets. The F3-8PEGA-Ce6 NCs also displayed good biocompatibility *in vitro* and their constituent composition, as well as previous biodistribution studies, make us believe that this will remain true *in vivo*. 8PEGA additionally demonstrated clear promise as a molecular imaging agent in MRI when coupled with techniques meant to suppress water and fat signals. Overall the F3-8PEGA-Ce6 presents an attractive universal NC for theranostics (imaging and PDT), from heart arrhythmia to cancer, and possibly to other pathologies. The potential benefits of rapid renal clearance and of accumulation in early stage tumors, even before angiogenesis, coupled with the MRI results, encourage a translation to animal studies.

3.5 Acknowledgments

We acknowledge support from the US National Inst. Of Health, NIH grant R01CA186769 (RK). We also acknowledge the NSF MRI-ID grant DBI-0959823 (Nils G. Walter PI) for seeding the Single Molecule Analysis in Real-Time (SMART) Center, which enabled the microscopy experiments, and the University of Michigan Microscopy and Image Analysis Laboratory for gathering TEMs.

3.6 Materials and Methods

Materials: Chlorin e6 (Ce6) and 1-Ethyl-3-(3-dimethylaminopropyl)carbodiimide (EDC) are sourced from Frontier Scientific. 8PEGA (40kDa) and Bi-PEG (Maleimide-PEG-Succinimydal Ester, 2kDA) is sourced from Creative PEG Works. F3-Cys peptide (KDEPQRRSARLSAKPAPPKPEPKPKKAPAKKC) is sourced from SynBioSci. 190 proof natured ethanol from Decon Labs. 10kDa and 300kDa filters for Amicon Cells and 10kDa centrifugal filters are sourced from Amicon. DMEM [(+) glutamine, sugar, sodium pyruvate), penicillin streptomycin, and fetal bovine serum are sourced from Life Technologies. All other chemicals sourced from Sigma Aldrich. Acrylamide, 3-(Acryloyloxy)-2-hydroxypropyl methacrylate (AHM), aminopropyl methylacrylamide hydrogen chloride salt (APMA), N-hydroxy succinimide (NHS), N,N'-Dicyclohexylcarbodiimide (DCC), Brij L4, dioctyl sulfosuccinate sodium salt (AOT), dimethyl sulfoxide (DMSO), dimethyl formamide (DMF), ammonium persulfate (APS), tetramethyl ethylene diamine (TEMED), phosphate buffer saline (0.01M, PBS), hexanes, cysteine, anthracene dipropionic acid (ADPA), calcein AM, propidium iodide (PI).

8PEGA-Ce6 Conjugate: Ce6 is conjugated to 8PEGA *via* DCC/NHS coupling in DMF.[14] Briefly, 448uL of Ce6 solution (20mg/mL, DMF) is activated with 154.8uL DCC and 172.8uL NHS under stirring (20mg/mL, DMF) for 30 minutes. 500mg 8PEGA is solvated in DMF at a concentration of 50mg/mL using sonication. Upon solvation, the Ce6 solution is added to the 8PEGA solution and allowed to stir overnight. The following day, unconjugated Ce6 is removed using 50% ethanol/PBS mixture in an Amicon Cell filtration system using a 10kDa membrane. After purification, the solvent is exchanged with Millipore ultrapure water, the materials filtered using a 0.45um syringe filter, and freeze dried for storage.

F3-8PEGA-Ce6 Conjugate: 8PEGA-Ce6 was modified with F3 *via* the same methods reported by our lab over the years.[15,20-23] After modification with F3-cys, the UV/VIS was then taken to ensure that the Ce6 had not aggregated in the process. Briefly, 20mg of Bi-PEG is added to 1mL of 8PEGA-Ce6 (20mg/mL, PBS) and stirred for 30 minutes. The solution is then washed 4x15mintues in PBS using a 10kDa centrifugal filter. The resulting solution is concentrated to 20mg/mL (by original mass), 22mg of F3-cys is added (220uL, 11mg/110uL DMSO), and left to stir over night. The next day, excess of cysteine is added and stirred for 2 hours to cap any unreacted maleimide groups. The solution is then filtered again using a 10kDa centrifugal filter and millipore ultrapure water, and freeze dried for storage.

Ce6 Encapsulated Polyacrylamide Nanoparticles (PAAm NPs): Ce6 is encapsulated in PAA NPs through a slightly modified previously reported method.[17] Briefly, 5mg of Ce6 is added to 930uL of PBS and 100uL DMSO with 28mg APMA, 19mg NHS, and 16mg EDC. The solution is stirred at 37 ^{o}C for 2 hours. Acrylamide and AHM are then added to the solution (368mg and 52.6uL, respectively) and sonicated to create a uniform solution. This solution is added to a 100mL round bottom flask containing 31mL hexanes, 2.2mL Brij L4, and 1.07g AOT

under stirring. The stirring is adjusted to where the generated vortex is just barely touching the stir bar (~500 RPM). The contents of the flask are then purged with nitrogen for 15 minutes. Nitrogen flow is removed from contact with the flask contents and maintained inside the flask. 15mg of APS in 100uL of water is added dropwise to initiate polymerization and 100uL of TEMED added dropwise to catalyze the process. Polymerization is allowed to proceed for 2 hours. Hexanes are then removed *via* rotary evaporation. The resulting contents are re-dispersed in ethanol and cleaned using 10x150mL ethanol and 5x150mL Millipore ultrapure water in an Amicon Cell using a 300kDa filter. The purified materials are syringe filtered using a 0.45um filter and freeze dried for storage.

Equipment: A Shimadzu UV-1601 UV/Visible Spectrophotometer is used for recording and adjusting the optical density (OD) of PAAm-Ce6 NPs. All fluorescence spectra are taken using a Fluoromax-3.

Size Analysis: Size of 8PEGA was characterized through two methods: TEM and NMR. To gather images of 8PEGA in its hydrated form, the compound was deposited on a copper grid, stained with uranyl acetate, and placed into the chamber while the grid is still wet. This enabled reasonable visualization of the low electronically dense 8PEGA by using surface tension to maintain its conformation. Size was analyzed via NMR using the Stokes-Einstein equation for translational motion (see MRI section for NMR measurements).

MRI: NMR relaxation times T_1, T_2 and translational diffusion constant, D, of 8PEGA were determined at 25 and 35 °C with a Varian/Agilent 16.4T NMR high resolution spectrometer equipped with pulsed field gradients. T_1, T_2 and diffusion data were collected with inversion-recovery, spin-echo, and stimulated-echo pulse sequences, respectively.

T_1 times were estimated by fitting recovery of longitudinal magnetization to $M_z(t) = M_0(1 - 2\exp\left(-\frac{t}{T_1}\right))$ where t is the time between the inversion RF pulse and sampling RF pulse. T_2 times were estimated by fitted decay of transverse magnetization to $M_{xy}(t) = M_{xy}(0)\exp\left(-\frac{t}{T_2}\right)$ where t is the time for formation of the spin echo. The translation diffusion constant D was estimated by fitting the decay of magnetization due to a pair of pulsed magnetic field gradients in a stimulate echo experiment to $M_{xy}(b) = M_0\exp(-bD)$ where b is given by $b(G_z, \delta, \Delta) = (\gamma G_z \delta)^2(\Delta - \frac{\delta}{3})$ where G_z amplitude of the applied gradient, γ is the proton gyromagnetic ratio, is the, δ is the duration of the applied gradient and Δ is the time separation between the gradient pair.

Relaxation times and diffusion constant were estimated by fitting appropriate exponential functions to the NMR data using scripts written in Matlab (The Mathworks, Natick, MA). MRI was performed with a Varian/Agilent 7T animal imaging system using a 120mm diameter shielded gradient set capable of 400mT/m and a 40mm millipede RF coil. The images were created with a diffusion-weighted, spin-echo sequence with TR/TE of 500/200ms and b values of 10^8 and 10^{10} s/m^2 for Figures 6A and 6B, respectively.

Reactive Oxygen Species (ROS) Evaluation: We use the so called "*k-value*" test, a method of relatively quantifying the amount of ROS produced (larger *k-value* = more ROS).[12] The 8PEGA-Ce6 ROS k-value was previously reported at an OD of 0.12 at 661nm.[14] To establish comparable *k-values*, the PAAm-Ce6 NPs are normalized to the OD of 8PEGA-Ce6 reported data (adjusted to OD = 0.12 at 660nm) and the k-value evaluated *via* the same means as previously reported.[12,14] Briefly, 80 uL of ADPA (0.3 mg/mL) is added to 2 mL of OD = 0.12 PAAm-Ce6 NPs in PBS. The fluorescence of ADPA is taken before illumination with 661nm

light and recorded at 427nm; this is repeated after every 300 seconds with 661nm illumination. The ADPA 427nm data points are then plotted as $\ln(I/I_o)$ vs. time, where the slope is the resulting k-value.

Cell Culture PDT Test: HeLa 229 cells are chosen as the cancer cell test line due to their robust nature. These cells were grown using DMEM culture medium containing 1% PenStrep and 10% fetal bovine serum. An arc lamp was used as the excitation source for PDT and control tests. Briefly, a 35mm culture dish is seeded with 100,000 cells and incubated with 200 ug/mL F3-8PEGA-Ce6 for 2 hours. For the cell live/dead tests the cells are stained using calcein AM green. After incubation, the cells are washed 3 times with pre-warmed Dulbecco's PBS (DPBS) and 1mL of pre-warmed colorless DMEM (no serum) is added. A 20 uL solution of propidium iodide (1 mg/mL) is added as a necrotic cell death indicator for evaluating the PDT.

Confocal imaging was performed using an ISS ALBA time-resolved confocal microscope, with an IX-81 Olympus microscope body and a U-Plan S-APO 60X 1.2NA water immersion objective. A Fianium supercontinuum laser with an acousto-optical filter was used to generate picosecond-excitation pulses at a wavelength of 488nm at a repetition rate of 20 MHz. Fluorescent emission was separated into two channels by a 592nm shortpass dichroic mirror and collected simultaneously through 100um pinholes and a 531 +/- 20nm bandpass filter (calcein channel) and a 630 ± 32nm bandpass filter (propidium iodide channel) onto a low noise avalanche photodiode.

Photodynamic therapy was activated using a mercury arc lamp with a 692+/-20nm excitation filter, using neutral density filters to adjust the total incident power to 50mW/cm^2.

3.7 References

[1]Hopkins, T.; Swanson, S.D.; Hoff, J.D.; Potter, N.; Ukani, R.; Kopelman, R. An Ultra-Compact Nano-theranostic PEG Platform for Cancer and Heart Arrythmia. *ACS Appl. Bio Mater.*, In submission.

[2]Dougherty TJ, Gomer CJ. Introduction. *Lasers Surg. Med.*, 2011, **43**, 541.

[3]Bernstein et al. Photopheresis in HIV-1 infected patients utilizing Benzoporphyrin derivative Verteporfin/BPD-MA and light. *Curr. HIC Res.*, 2007, **6**, 152 – 63.

[4]J. Harrell and R. Kopelman. Biocompatible probes measure intracellular activity. *Biophotonics Int.*, 2000, **7**, 22 – 24.

[5]Gupta et al. Multifunctional Nanoplatforms for Fluorescence Imaging and Photodynamic Therapy Developed by Post-loading Photosensitizer and Fluorophore to Polyacrylamide Nanoparticles. *Nanomed. Nanotech. Biol. Med.*, 2012, **8**, 941 – 50. DOI: 10.1016/j.nano.2011.11.011.

[6]Xu, H.; Buck, S.M.; Kopelman, R.; Philbert, M.A.; Brasuel, M.; Ross, B.D.; Rehemtulla, A. Photo-Excitation Based Nano-Explorers: Chemical Analysis Inside Live Cells and Photodynamic Therapy. *Israel J. of Chem.*, 2004, **44**, 317 – 37. DOI: 10.1560/WA5H-KBGV-PR13-NEVN

[7]Koo et al. Multifunctional Nanoparticle Platforms for In Vivo MRI Enhancement and Photodynamic Therapy of a Rat Brain Cancer. *J. Magn. Magn. Mater.*, 2005, **293**, 404 – 10. DOI: 10.1016/j.jmmm.2005.02.061

[8]Pandey, R.K.; Goswami, L.N.; Chen, Y.; Gryshuk, A.; Missert, J.R.; Oseroff, A.; Dougherty, T.J. Nature: a rich source for developing multifunctional agents. Tumor-imaging and photodynamic therapy. *Lasers Surg. Med.*, 2006, **38**, 445 – 67. DOI: 10.1002/lsm.20352.

[9]Koo, Y.E.; Reddy, G.R.; Bhojani, M.; Schneider, R.; Philbert, M.A.; Rehemtulla, A.; Ross, B.D.; Kopelman, R. Brain cancer diagnosis and therapy with nanoplatforms. *Advanced Drug Delivery Reviews*, 2006, **58**¸1556 – 77. DOI: 10.1016/j.addr.2006.09.012

[10]Reddy et al. Vascular Targeted Nanoparticles for Imaging and Treatment of Brain Tumors. *Clin. Cancer Res.*, 2006, **12**, 6677 – 86. DOI: 10.1158/1078-0432.CCR-06-0946.

[11]Baba, K.; Pudavar, H.E.; Roy, I.; Ohulchanskyy, T.Y.; Chen, Y.; Pandey, R.; Prasad, P.N. A New Method for Delivering a Hydrophobic Drug for Photodynamic Therapy Using Pure Nanocrystal Form of the Drug. *Mol. Pharm.*, 2007, **4**, 289 – 97. DOI: 10.1021/mp060117f.

[12]Moreno, M.J.; Monson, E.; Reddy, R.G.; Rehemtulla, A.; Ross, B.D.; Philbert, M.; Schneider, R.J.; Kopelman, R. Production of Singlet Oxygen by $Ru(dpp)SO_3)_2)_3$ Incoproated in Polyacrylamide PEBBLES. *Sensor Actuat. B-chem.*, 2003, **90**, 82 – 9. DOI: 10.1016/S0925-4005(03)00057-1.

[13]Roy, I.; Ohulchanskyy, T.Y.; Pudavar, H.E.; Bergey, E.J.; Oseroff, A.R.; Morgan, J.; Dougherty, T.J.; Prasad, P.N. Ceramic-based nanoparticles entrapping water-insoluble photo-sensitizing anticancer drugs: A novel drug-carrier system for photodynamic therapy. *J. Am. Chem. Soc.*, 2003, **26**, 7860 – 5. DOI: 10.1021/ja0343095.

[14]Avula et al. Cell-selective Arrhythmia Ablation for Photomodulation of Heart Rhythm. *Sci. Trans. Med.*, 2015, **7**, 311ra172. DOI: 10.1126/scitranslmed.aab3665.

[15]Karamchand, L.; Kim, G.; Wang, S.; Hah, H.J.; Ray, A.; Jiddou, R.; Lee, Y.E.k.; Philbert, M.A.; Kopelman, R. Modulation of Hydrogel Nanoparticle Intracellular Trafficking by Multivalent Surface Engineering with Tumor Targeting Peptide. *Nanoscale*, 2013, **5**, 10327. DOI: 10.1039/c3nr00908d.

[16]Watanabe et al. Nucleolin as Cell surface Receptor for Tumor Necrosis Factor-α Inducing Protein: A Carcinogenic Factor of *Helicobacter Pylori*. *J. Cancer Res. Clin. Oncol.*, 2010, **136**, 911 – 21. DOI: 10.1007/s00432-009-0733-y.

[17]Hopkins, T.; Ukani, R.; Kopelman, R. Intracellular Photodynamic Activity of Chlorin e6 Containing Nanoparticles. *Int. J. Nanomed. Nanosurg.*, 2016, **2**, 119. DOI: 10.16966/2470-3206.

[18]Lechner, M.D.; Machtle. Characterization of Nanoparticles. *Macromol. Symp.*, 1999, **145**, 1 – 7.

[19]Calicetic, P.; Salmaso, S. Stealth Properties to Improve Therapeutic Efficacy of Drug Nanocarriers. *J Drug Deliv.*, 2013, DOI: 10.1155/2013/374252.

[20]Hah, H.J.; Kim, G.; Lee, Y.E.; Orringer, D.A.; Sagher, O.; Philbert, M.A.; Kopelman, R. Methylene Blue-Conjugated Hydrogel Nanoparticles and Tumor-Cell Targeted Photodynamic Therapy. *Macromol. Biosci.*, 2011, **11**, 90 – 9. DOI: 10.1002/mabi.201000231.

[21]Nie et al. Hydrogel Nanoparticles with Covalently Linked Coomassie Blue for Brain Tumor Delineation Visible to the Surgeon. *Small*, 2012, **8**, 884 – 91. DOI: 10.1002/smll.201101607.

[22]Henke et al. Peptide-conjugated antisense oligonucleotides for targeted inhibition of a transcriptional regulator *in vivo*. *Nature Biotechnol.*, 2008, **26**, 91 – 100. DOI: 10.1038/nbt1366.

[23]Winer, I.; Wang, S.; Lee, Y.E.; Fan, W.; Gong, Y.; Burgos-Ojeda, D.; Spahlinger, G.; Kopelman, R.; Buckanovich, R.J. F3-Targeted Cisplatin-Hydrogel Nanoparticles as an Effective Therapeutic That Targets Both Murine and Huamn Ovarian Tumor Endothelial Cell *In vivo*. *Cancer Res.*, 2010, **70**, 8674 – 83. DOI: 10.1158/0008-5472.CAN-10-1917.

[24]Aluigi et al. Chlorin e6 keratin nanoparticles for photodynamic anticancer therapy. *RSC Adv.*, 2016, **6**, 33910 – 18. DOI: 10.1039/C6RA04208B.

[25]Bharathiraja, S.; Moorthy, M.S.; Manivasagan, P.; Seo, H.; Lee, K.D.; Oh, J. Chlorin e6 conjugated silica nanoparticles for targeted and effective photodynamic therapy. *Photodiagnosis Photodyn. Ther.*, 2017, **19**, 212 – 20. DOI: 10.1016/j.pdpdt.20172.06.001.

[26]Bharathiraja, S.; Manivasagan, P.; Moorthy, M.S.; Bui, N.Q.; Lee, K.D.; Oh, J. Chlorin e6 conjugated copper sulfide nanoparticles for photodynamic combined photothermal therapy. *Photodiagnosis Photodyn. Ther.*, 2017, **19**, 128 – 34. DOI: 10.1016/j.pdpdt.2017.04.005.

[27]Hou, W.; Xia, F.; Alves, C.S.; Qian, X.; Yang, Y.; Cui, D. MMP2-Targeting and Redox-Responsive PEGylated Chorin e6 Nanoparticles for Cancer Near-Infrared Imaging and Photodynamic Therapy. *ACS Appli. Mater. Interfaces*, 2016, **8**, 1447 – 57. DOI: 10.1021/acsami.5b10772.

[28]Zhang, D.; Wu, M.; Zeng, Y.; Wu, L.; Wang, Q.; Han, X.; Liu, X.; Liu, J. Chlorin e6 Conjugated Poly(dopamine) Nanospheres as PDT/PTT Dual-Modal Therapeutic Agents for Enhanced Cancer Therapy. *ACS Appl. Mater. Interfaces*, 2015, **7**, 8176 – 87. DOI: 10.1021/acsami.5b01027.

[29]Pezzella, F.; Gatter, K.C. Evidence Showing That Tumors Can Grow Without Angiogenesis and Can Switch Between Angiogenic and Nonangiogenic Phenotypes. *J. Natl. Cancer. Inst.*, 2016, **108**. DOI: 10.1093/jnci/djw032.

[30]Alvares, R.D.A.; Lau, J.Y.C.; Macdonald, P.M.; Cunningham, C.H.; Prosser, R.S. Direct Quantitative ^{13}C-Filtered ^{1}H Magnetic Resonance Imaging of PEGylated Biomacromolecules In Vivo. *Magn. Reson. Med.*, 2017, **77**, 1553 – 61. DOI: 10.1002/mrm.26237.

[31]Bieze, T.W.N.; van der Maarel, J.R.C.; Eisenbach, C.D.; Leyte, J.C. Polymer Dynamics in Aqueous Poly(ethylene oxide) Solutions. *Macromolecules*, 1994, **27**, 1355 – 66.

[32]Stejskal, E.O.; Tanner J.E. Spin Diffusion Measurements: Spin Echoes in the Presence of a Time-Dependent Field Gradient. *J. Chem. Phys.*, 1965, **42**, 288.

Chapter 4: Multifuctional Pluronic Micelles for Choroidal Neovascularization (CNV) Treatment

4.1 Introduction

The following is in preparation for submission to *Future Medicine – Nanomedicine*.

It has been shown in the literature that combining cancer ablating modalities (e.g. combinations of chemo, photodynamic therapy, or photothermal therapy)[2-7] are more potent than any modality that is applied alone. Photodynamic therapy (PDT) and photothermal therapy (PTT) are considered the most promising in terms of cell selectivity due to the necessity of externally applied light to trigger their cell ablating properties, compared to chemo drugs that are always active or radiation therapy that is non-selective.[8] Cell selectivity can be further increased *via* delivery of the dyes to cancer cells using targeted nanoparticles (NPs). Combinations of PDT/PTT in targeted NPs have already been reported.[9,10]

Choroidal Neovascularization (CNV) is a condition that if left untreated in the eyes will lead to blindness. Current methods of treatment involve the use of growth factor inhibitors that are delivered intravitreally[11] or untargeted PDT using Verteporfin (VP).[12] Strictly speaking, CNV is not a form of cancer since it only involves de-regulated angiogenesis. However, it can be considered very similar to cancer since it is an uncontrolled growth of a cell population that leads to detrimental biological effects (blindness) and possesses a leaky vasculature.[13] This leaky vasculature indicates that NP-mediated delivery of photosensitizers (PSs) for PDT or PTT would be highly effective due to the Enhanced Permeability and Retention (EPR) effect, the same principle and method NPs take advantage of in cancer.[14] In addition, as the detrimental tissue is

entirely composed of vasculature, there is no danger of hypoxia, and the eye is mostly transparent, allowing for highly viable PDT. Cationic liposomes have previously been used to encapsulate VP and were shown to have greater PDT efficacy than the free dye.[15]

Due to the above information, previously reported pluronic micelles[16] containing the FDA-approved dyes VP and indocyanine green (ICG) have been designed for improved treatment of CNV. Verteporfin will be used for PDT and ICG may induce combined PTT effects with PDT, provide photoacoustic imaging, and/or fluorescence imaging. The micelles may also be functionalized with polyethylene glycol (PEG) and a cysteine terminated targeting peptide to increase accumulation in the anomalous vasculature of CNV.[16]

4.2 Results

4.1.1 UV/VIS and Fluorescence of Micelles: Figures 4-1 and 4-2 are UV/VIS spectra of the pluronic micelles prepared 1) with VP and ICG separately, 2) with VP and ICG together, and 3) the two spectra added together. As their general shapes remain the same, the spectra show that the dyes do not interfere with each other, as demonstrated by the simple additive properties of the spectra. Filtration of the micelles through a 100 kDa centrifugal filter yielded no loss of color, indicating that the dyes are trapped entirely within the micelles. This is further reinforced by the red shift of the ICG peak from 780nm to 797nm, a common feature of the dye when solvent effects are removed (in this case, via encapsulation in the micelles' hydrophobic interior). In addition, no aggregates seem to be present by a lack of dimer peaks in the UV/VIS.

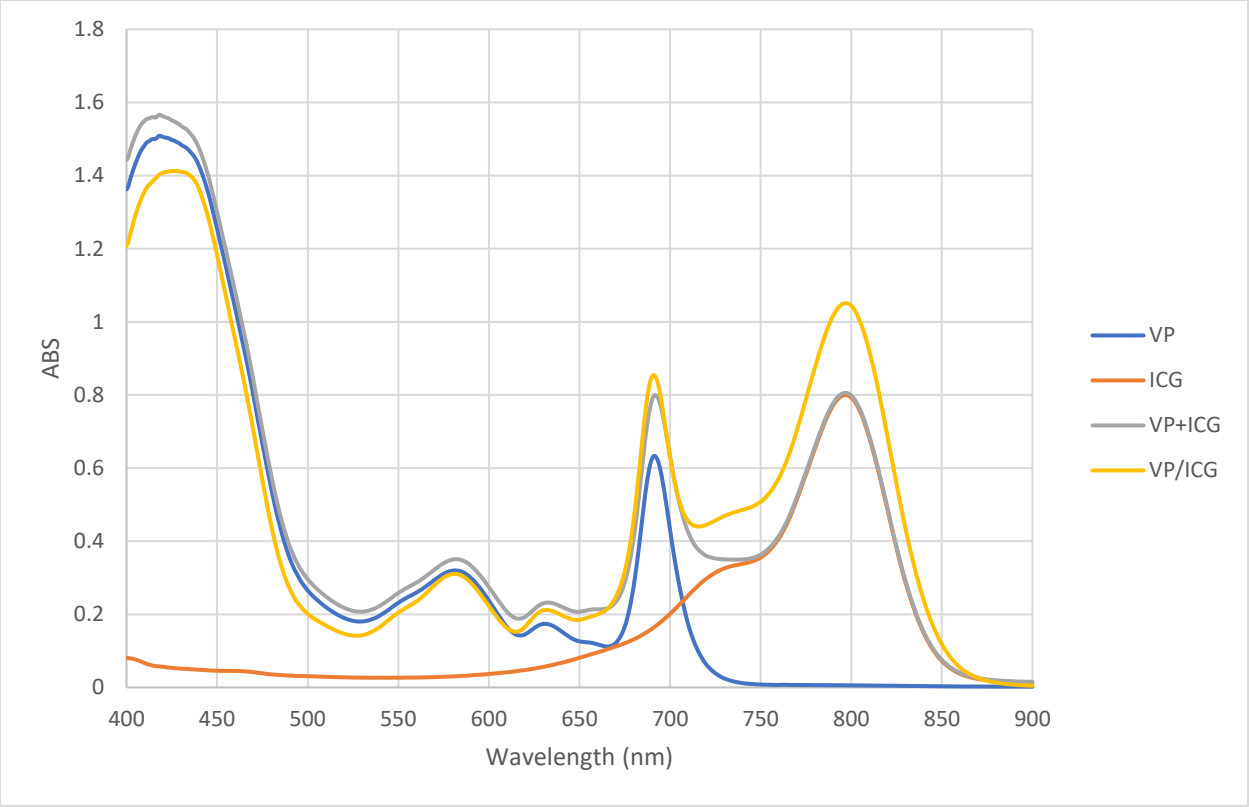

Figure 4-1: Absorption spectra of pluronic micelles in pure water (2mg/mL) containing either VP (blue) or ICG (orange) alone and the two spectra added together (grey). Yellow is the spectrum of the as-prepared and used micelles.

Fluorescence spectra of the pluronic micelles containing both VP (Figure 4-2) and ICG (Figure 4-3) were taken to demonstrate preservation of optical properties. ICG was excited using the red shifted 797nm peak. Porphyrin dyes are known to have exceptionally small stokes shifts, and so to capture the peak fluorescence point VP was excited at 400nm.

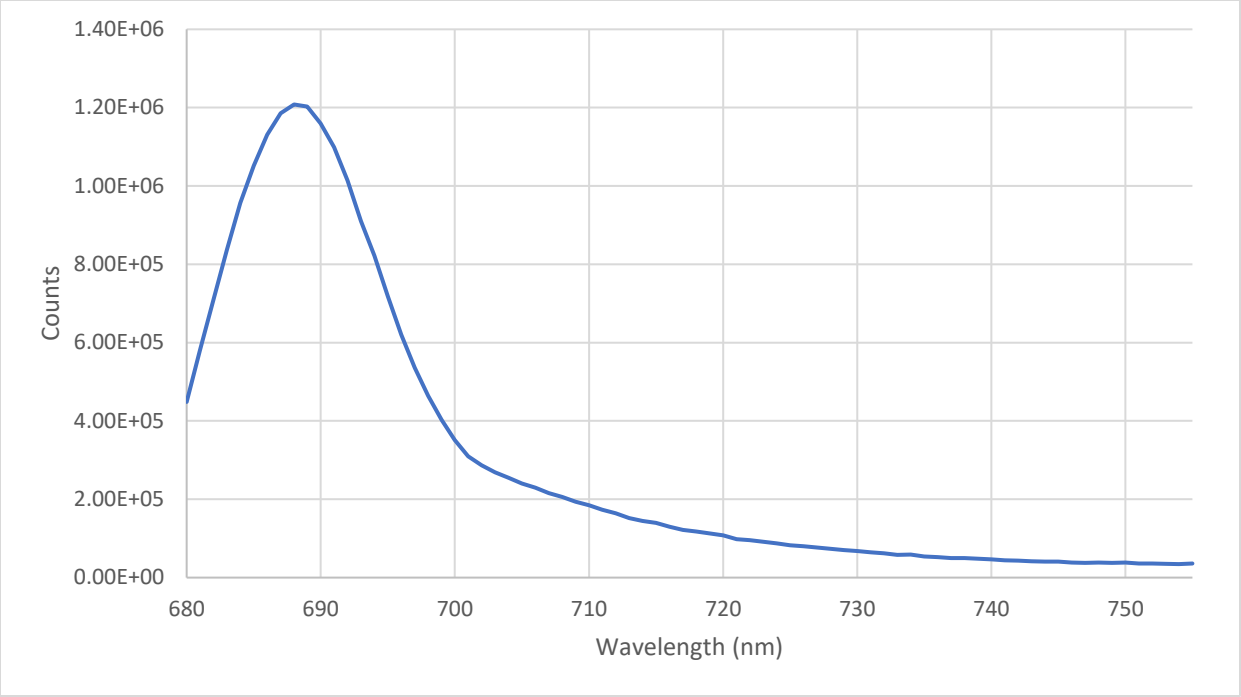

Figure 4-2: Fluorescence spectra of VP in pluronic micelles containing both VP and ICG. Concentration is 1mg/mL micelles in pure water. Excited at 400 nm.

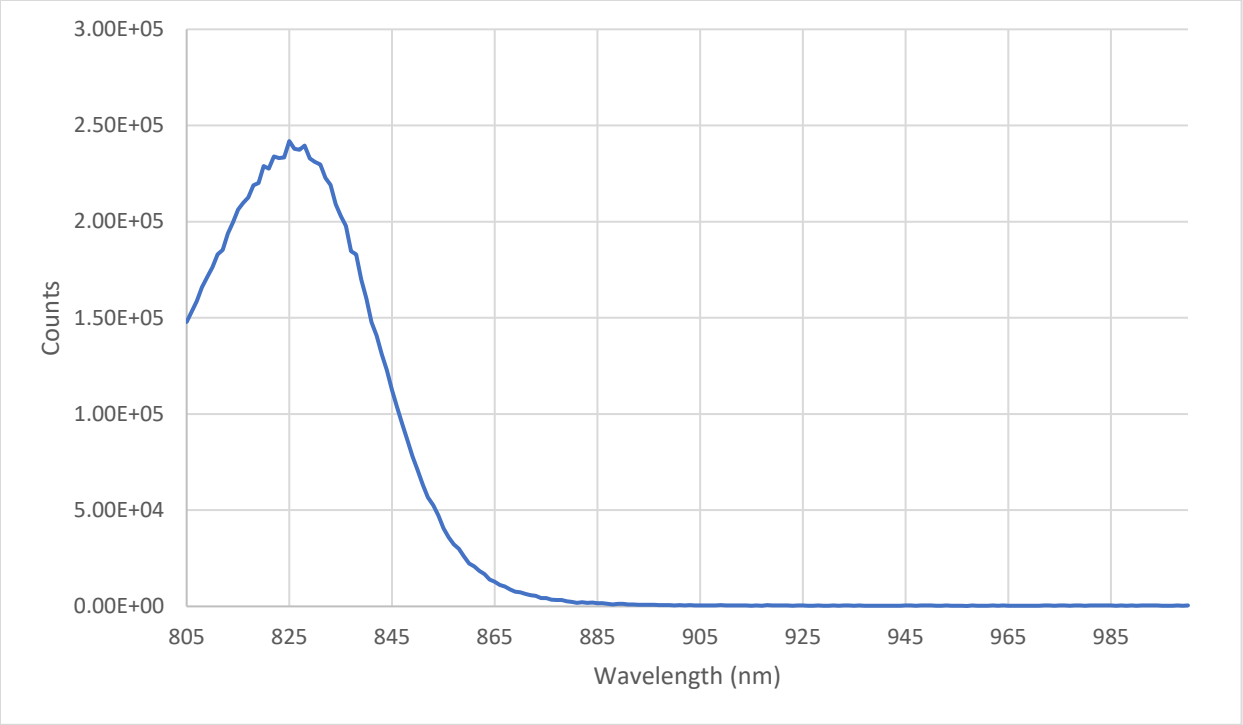

Figure 4-3: Fluorescence spectra of ICG in pluronic micelles containing both VP and ICG. Concentration is 1mg/mL micelles in pure water. In correspondence with the red shifted absorption, the fluorescence is also red shifted ~20nm. Excited at 797nm.

4.2.2 Characterization of Micelle Size: NP related systems can have their sizes characterized through either dynamic light scattering (DLS) or TEM. In this case, both must be employed. DLS typically uses a 658nm line, which is absorbed by the micelles, making characterization of the dye containing micelles by this method impossible. Therefore, DLS of blanks were taken (Figure 4-4) and compared with wet TEMs of the dye containing micelles (Figure 4-5).

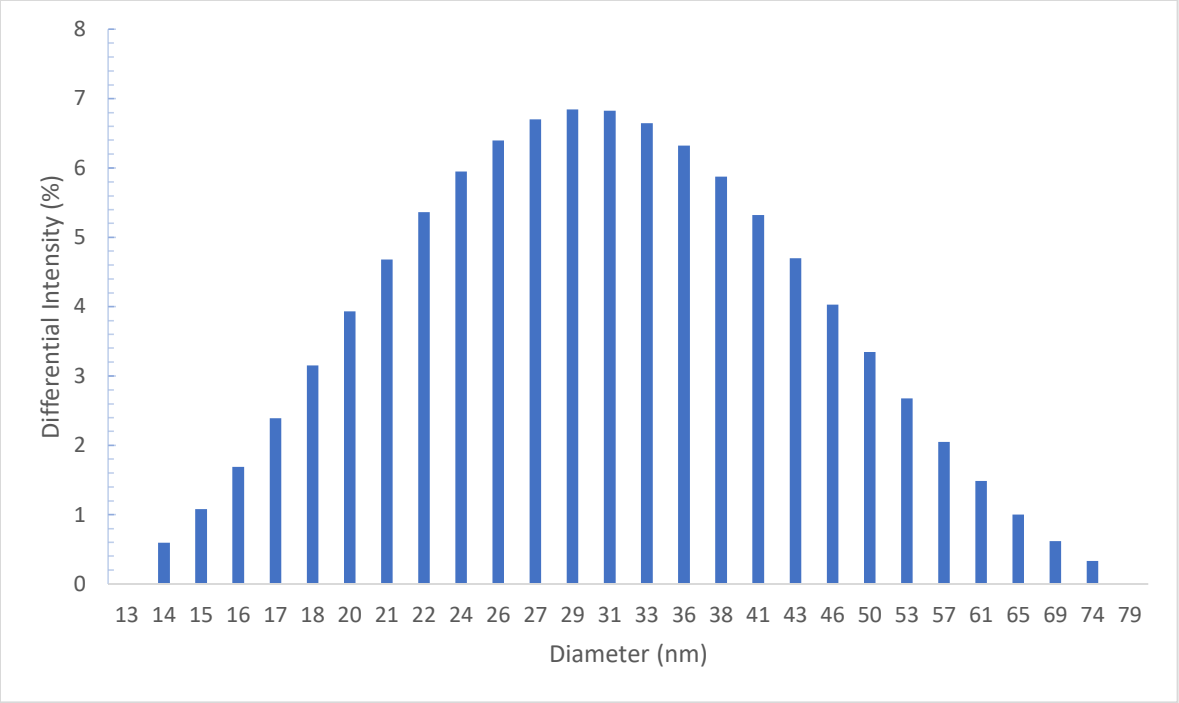

Figure 4-4: DLS measurement of blank micelles at 2mg/mL in pure water. Average size is found to be ~29nm.

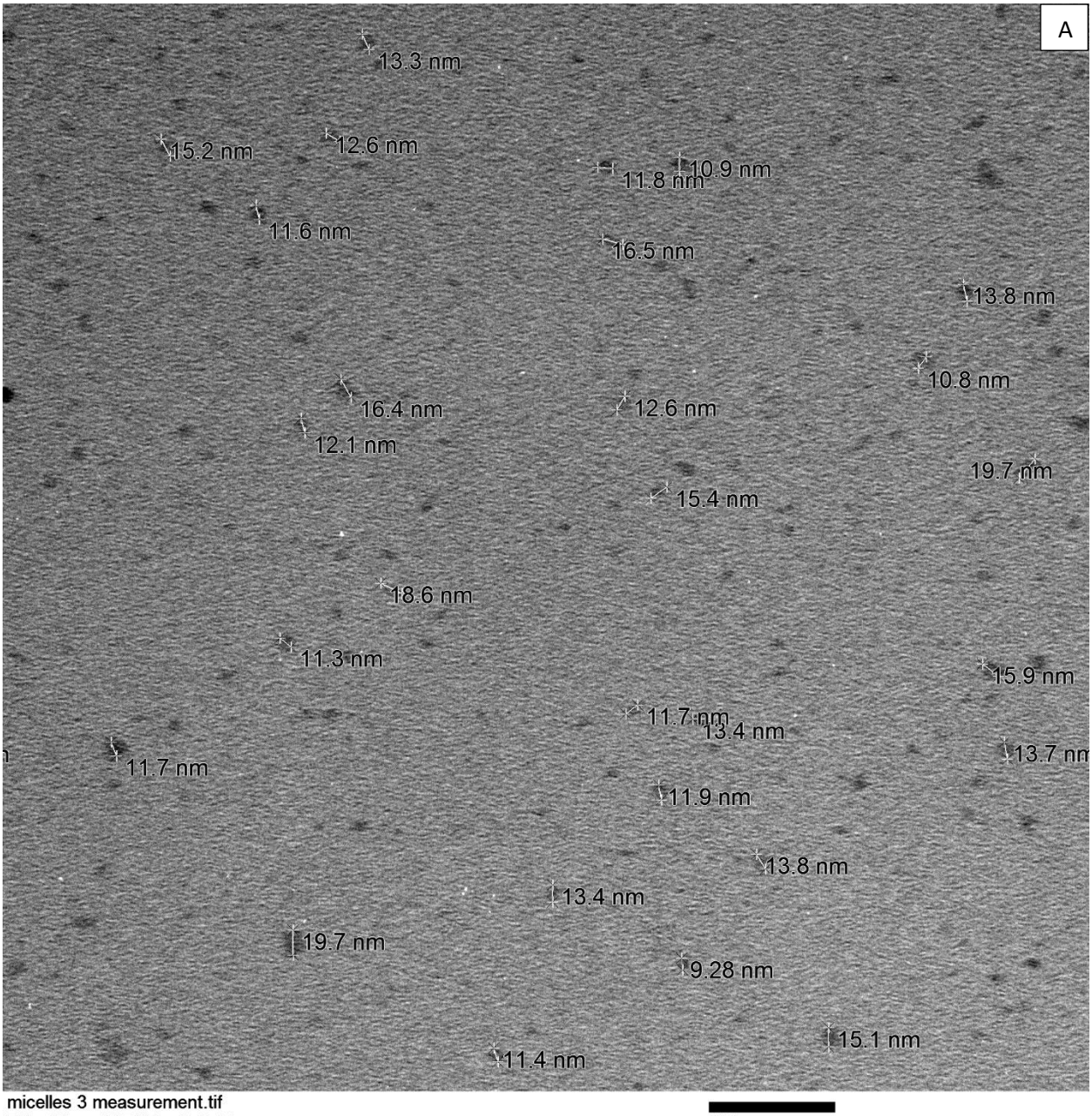
A
13.3 nm
15.2 nm
12.6 nm
11.8 nm
10.9 nm
11.6 nm
16.5 nm
13.8 nm
10.8 nm
16.4 nm
12.6 nm
12.1 nm
19.7 nm
15.4 nm
18.6 nm
11.3 nm
15.9 nm
11.7 nm
13.4 nm
13.7 nm
11.7 nm
11.9 nm
13.8 nm
13.4 nm
19.7 nm
9.28 nm
15.1 nm
11.4 nm
micelles 3 measurement.tif
Print Mag: 207000x @ 7.0 in
12:48:45 5/18/2018
100 nm
HV=89.0kV
Direct Mag: 30000x
Bottom Camera-MIL

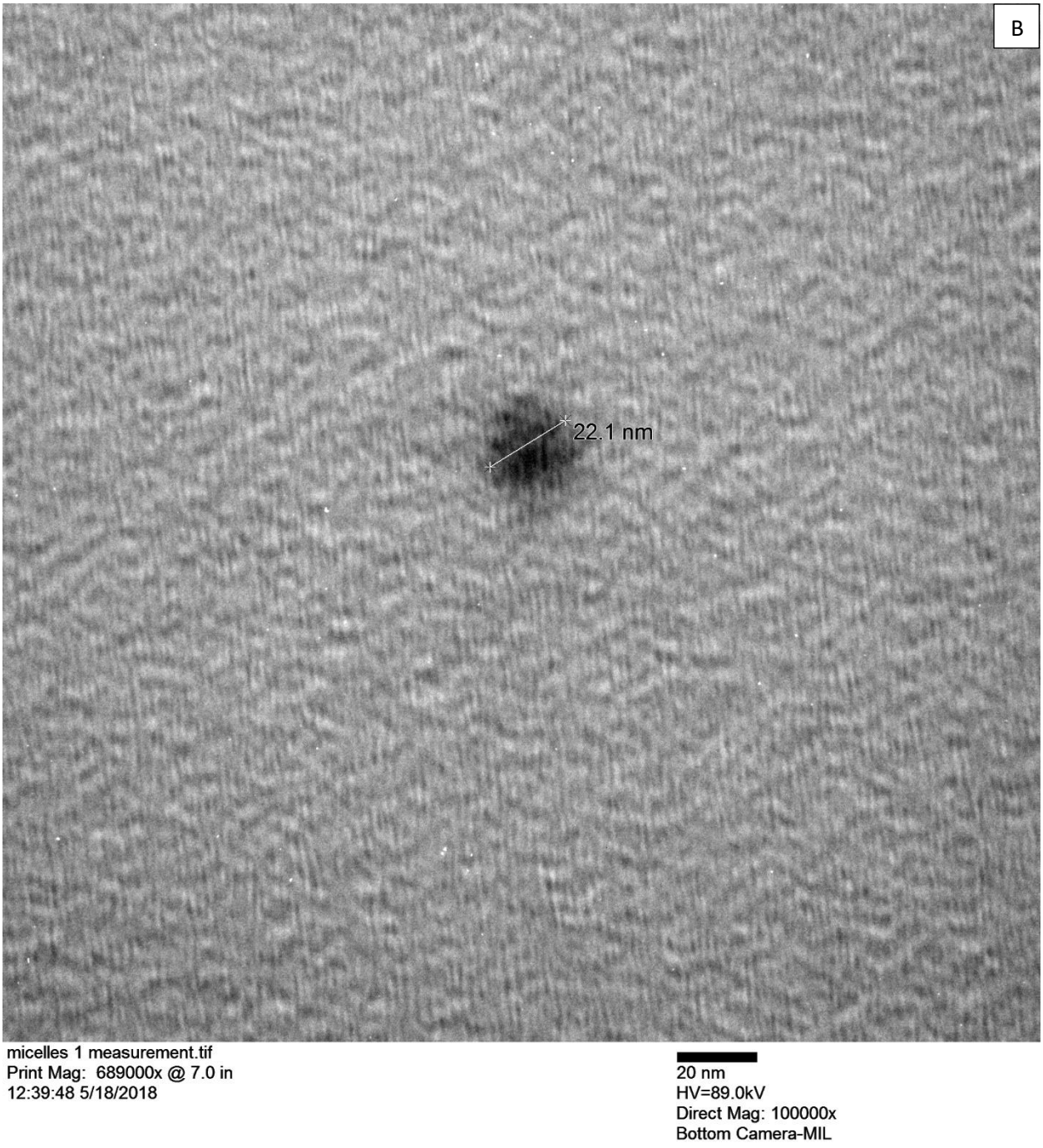

Figure 4-5: Wet TEM of pluronic micelles containing both VP and ICG. A) Wide field view of micelles on a copper grid. B) Zoomed in on a well resolved single micelle. Size distribution is predominantly in the range of 10-20nm.

4.2.3 Cytotoxicity of Micelles: Before proceeding to confocal microscopy studies, the biocompatibility of the as prepared micelles containing both VP and ICG was tested *via* MTT assay. HeLa cells were chosen as the test line and incubated overnight to allow adequate time for interaction with the micelles. The micelles displayed no toxicity at the high concentration of 200ug/mL, as shown by the essentially identical cell populations between the control and test lines after incubation (Figure 4-6).

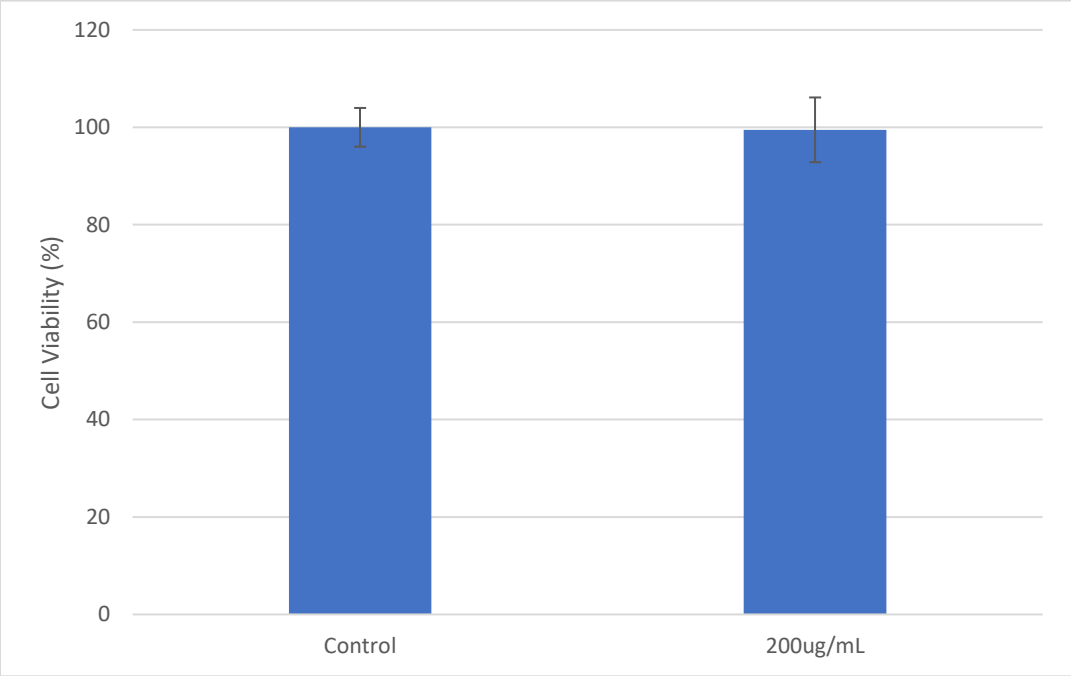

Figure 4-6: MTT assay of HeLa cells incubated with micelles containing both VP and ICG overnight.

4.2.4 Confocal Microscopy Evaluation of PDT: HeLa cells were taken for confocal microscopy to study the effects on the cells when initiating PDT at 690nm (Figure 4-7) or PTT at 780nm (Figure 4-8). Figures 4-7A/8A are cytosolic stain calcein AM fluorescence images of the cells prior to treatment and Figures 4-7B/8B are calcein AM after treatment. Membrane

impermeable propidium iodide (PI) stain was also employed to evaluate the damage to HeLa cells (Figures 4-7C/8C); no PI fluorescence is observable prior to treatment.

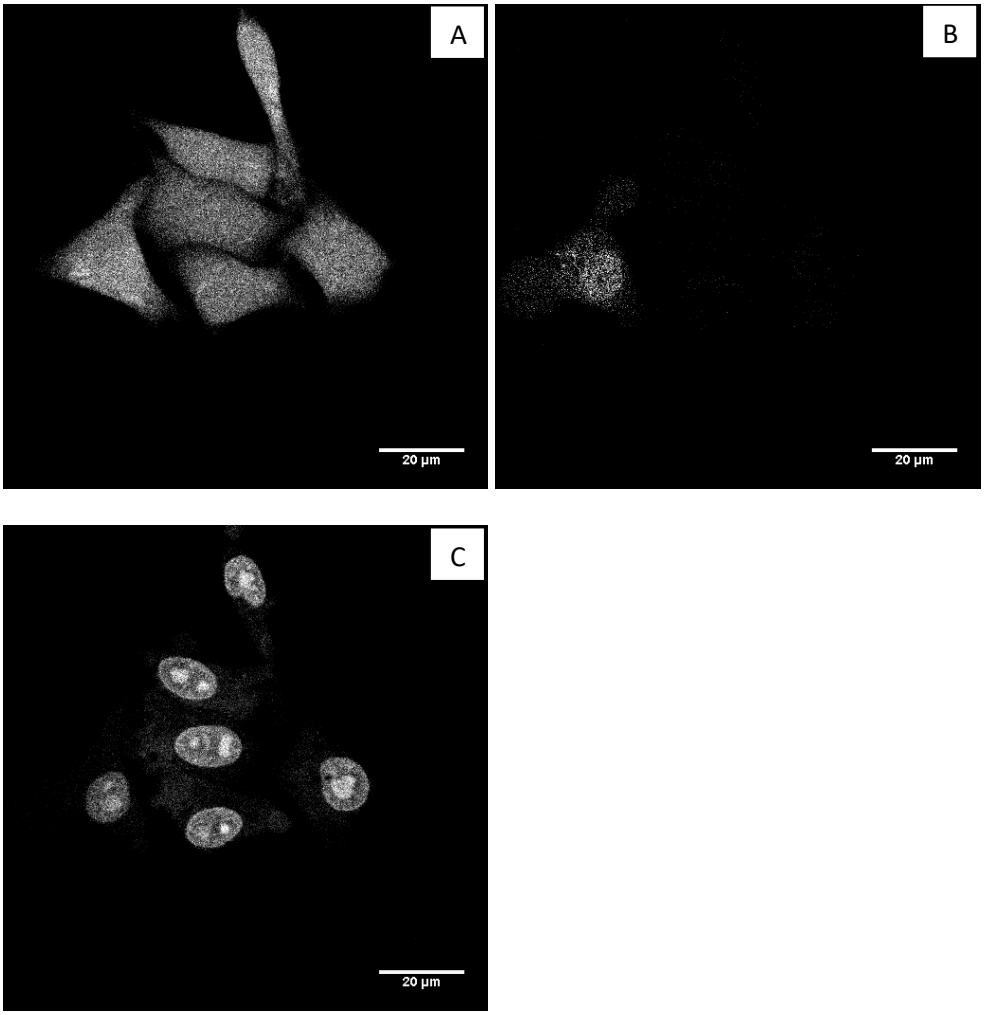

Figure 4-7: Confocal microscopy images of HeLa cells before and after VP-mediated PDT from VP/ICG containing micelles. A) Calcein AM fluorescence of cells prior to PDT. B) Calcein AM fluorescence after 10min of PDT (50mW/cm2, 690nm). C) PI fluorescence images after PDT.

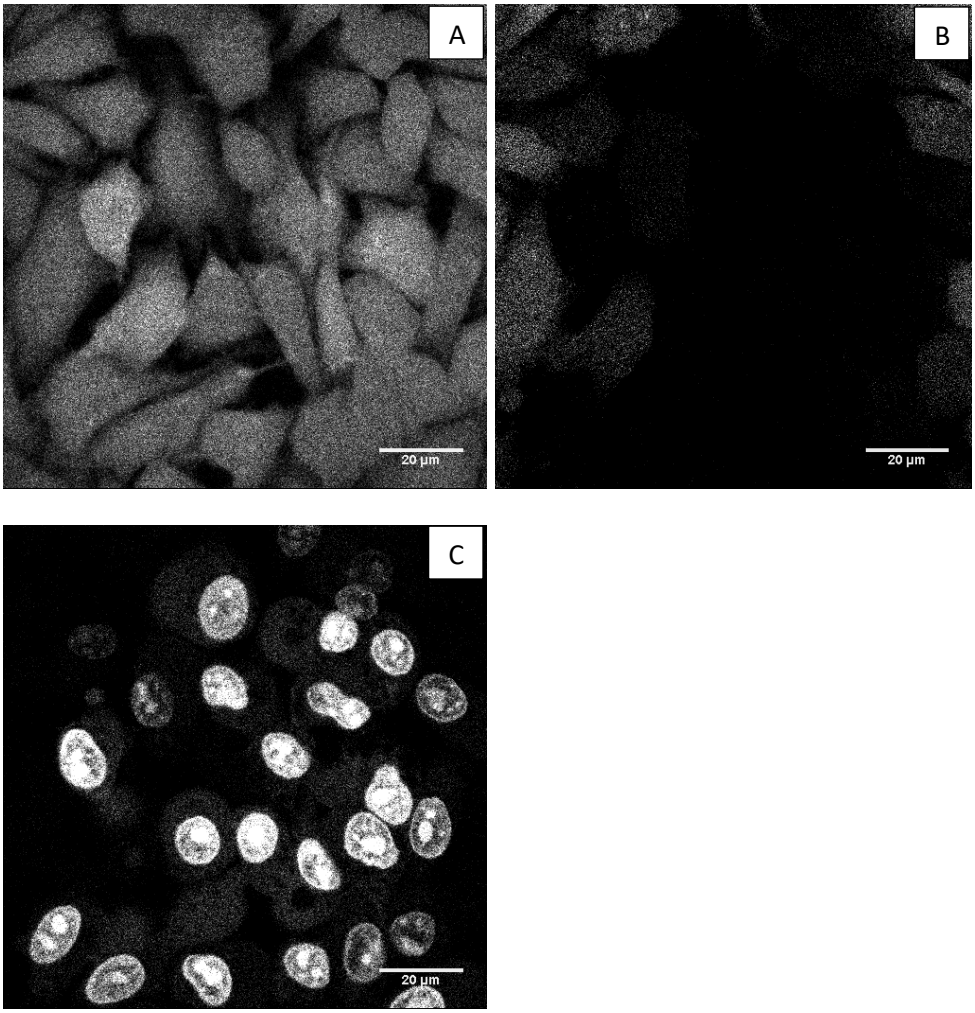

Figure 4-8: Confocal microscopy images of HeLa cells before and after ICG-mediated PTT from VP/ICG containing micelles. A) Calcein AM fluorescence of cells prior to PTT. B) Calcein AM fluorescence after 30min PTT (500mW/cm2, 780nm). C) PI fluorescence images after PTT.

4.3 Discussion

CNV is a difficult to treat condition due to a lack of existing methodologies that suitably target it while being highly selective. However, the anomalous and leaky vasculature make NP-mediated treatments an attractive improvement to resolving the condition.

Micelles constructed of the pluronics F68 and P123 very efficiently encapsulated the FDA-approved dyes ICG and VP when generated through the thin film rehydration method. The dyes VP and ICG were chosen for several reasons: 1) VP is specifically the PS FDA-approved for treatment of CNV via PDT, 2) ICG has also received FDA approval for fluorescence imaging in humans and absorbs deep tissue penetrating 780nm light, 3) ICG has been previously employed as either a photo-acoustic agent[17] or PTT agent.[18]

The absorption properties of the dyes are preserved and confirmed to be independent of each other by their simple additive nature (Figure 4-1). In addition, the dyes are still fluorescent, indicating that VP will still produce reactive oxygen species (ROS, Figure 4-2) and ICG will still function as a fluorescent imaging agent (Figure 4-3). ICG remaining fluorescent will not affect its ability to function as a photo-acoustic agent, as fluorescent ICG has been shown to be a capable agent in photo-acoustics already.[19] The absorption spectrum of the micelles used hereafter *in vitro* are shown in Figure 4-1 (yellow).

Size analysis of this system is difficult because they are micelles (problematic in TEM) and are broadband absorbers (prevent use of DLS). Therefore, a mixture of the two methods under modified conditions were necessary. Micelles with no dye enabled DLS (Figure 4-4) and TEM was measurable of micelles with both dyes by placing the copper grid into the microscope while wet; wet EM as used here took advantage of surface tension to allow some micelles on the grid to maintain their confirmation after the water evaporates in the vacuum chamber (Figure 4-5). It is found that the size of the micelles by DLS is ~29nm. TEM matches this well by ranging the 28 measured micelles to be between 10-20nm; it is expected that the micelles would be smaller by TEM, because though their structures are maintained by the surface tension, it is expected that the PEG blocks of the chain copolymer would still shrink somewhat from the

dehydration. The small size found here would benefit PDT *in vitro* due the enhanced surface area to volume ratio.

TEMs were taken in a two-week gap to explore their long-term stability. It is found that they are stable for at least two weeks when stored at 20mg/mL concentration. However, if they are stored at a dilute concentration of 1mg/mL for the same length of time, some degradation is observed. This is an expected result, as micelles form based on a concentration dependence, and so while they will be stable for a time at dilute working concentrations (i.e. reactions, *in vitro*), long term storage (weeks scale) should yield degradation.

To ensure viability in animal models, the cyto-toxicity of the micelles were tested via MTT assay (Figure 4-6). A virtual lack of any toxicity is observed in the tested HeLa cells at the high concentration of 200ug/mL, indicating that their application to animals, and eventually humans, should not pose any significant health concerns. In addition, F68 and P123 are materials composed of polypropylene glycol (PPG) and PEG, which are biodegradable, and so should quickly clear animals after treatment.

HeLa cells taken for testing PDT and PTT properties of the micelles showed significant promise. A very mild and low energy dosage of 690nm light to initiate PDT from VP resulted in the death of the tested HeLa cells, as shown by the significant decrease of calcein AM fluorescence due to loss of cytosolic contents (Figures 4-7A/B). ICG demonstrated similar effects under the *in vivo* safe energy dosage of 500mW/cm^2 (Figures 4-8A/B).

PI staining was additionally carried out to demonstrate the effects occurring were photo-mediated by the dyes, as PI is a membrane impermeable substance; for any staining to occur, physical rupture of the cell membranes must occur (Figures 4-7C/8C).

PDT was very quickly initiated and completed within 10min, however it should be noted that PTT required a substantially longer illumination period of 30min to occur. Given such a large time dosage was required, it would probably be desirable to increase the loading of the ICG to modulate the heating rate of the cells. However, this may also correspondingly decrease the PDT viability by VP due to transfer of excited state energy *via* FRET to ICG, quenching ROS production. This was shown to occur in liposomes containing the dyes Chlorin e6 and ICG.[20] PTT is also known to traditionally only cause necrosis in treated cells, leading to inflammation of the affected areas, which may be better off avoided in this case since the eyes are the target tissue.[20] Therefore, rather than performing PTT alone, it should always be in conjunction with PDT, where the treatment affects may be more quickly applied (combined PDT/PTT is known to be more efficient than either modality separately), achieving apoptosis with greater propensity or limit its role to imaging alone.

Although not performed here, F68 may be derivatized to be amine terminated, allowing for the grafting of PEG onto the micelles surfaces to increase blood circulation time and double as a molecular anchor for CNV targeting agents (e.g. RGD).[16,22]

4.4 Conclusion

Targetable, biocompatible micelles constructed of the pluronics F68 and P123 were successfully generated, encapsulating the FDA-approved dyes VP and ICG. Both dyes were capable of separately yielding cell death through PDT (VP) or PTT (ICG). ICG may also effectively function as an imaging agent through either fluorescence or photo-acoustics. These micelles are expected to enable highly selective treatment and imaging of CNV.

4.5 Acknowledgments

We acknowledge support from the US National Inst. Of Health, NIH grant R01CA186769 (RK). We also acknowledge the NSF MRI-ID grant DBI-0959823 (Nils G. Walter PI) for seeding the Single Molecule Analysis in Real-Time (SMART) Center, which enabled the microscopy experiments, and the University of Michigan Microscopy and Image Analysis Laboratory for gathering TEMs.

4.6 Experimental

Materials: Verteporfin is sourced from Active Biochem. USP Reference Standard Cardiogreen, Pluronic F68, Propdium Iodide (PI), 3-(4,5-dimethylthiazol-2-yl)-2,5-diphenyltetrazolium bromide (MTT), dimethylsulfoxide (DMSO), and methanol (99.8%, anhydrous) are sourced from Sigma Aldrich. Pluronic P123 is sourced from BASF. Calcein AM is sourced from Invitrogen and methylene chloride from Fisher Chemical.

Micelle Preparation: Micelles of pluronic F68 and P123 are constructed using a previously reported protocol.[16] Briefly, 84mg F68, 116mg P123, and 1.6mg VP are suspended in 5mL of methylene chloride in a 50mL round bottom flask. 500ug of cardiogreen in 1mL methanol is then added to the flask. The solvents are then removed using rotary evaporation to form a thin film and the contents allowed to sit overnight in a hood to ensure total removal of methylene chloride and methanol. The thin film is then rehydrated using 10mL of pure water and ultrasonication to form the micelles. The micelles are then filtered using a 0.45um polyether sulfone membrane. The shelf-life of the final suspension (20mg/mL micelles) is greater than 2 weeks as confirmed by TEMs of before and after.

Equipment: A Shimadzu UV-1601 UV/Visible Spectrophotometer is used for all absorption spectra. A Fluoromax 3 is used for all fluorescence spectra. Cell viability from MTT assay was measured using an Anthos 2010 plate reader.

Size Analysis: Micelles were characterized by TEM and DLS. Briefly, micelles containing no dye were used for DLS at a concentration of 2mg/mL in pure water. TEMs were taken through the Microscopy and Image Analysis Laboratory at the University of Michigan. TEM was carried out by depositing micelles on a copper grid and placing into the vacuum chamber while still wet. The purpose is that surface tension will cause the micelles to maintain their structure when the water evaporates, preventing some from simply collapsing due to the loss of hydration.

MTT Assay: A 24-well plate is seeded with 12,500 cells per well (4x2) and 600uL of DMEM (10% FBS, 1% Pen Strep). The cells are allowed to settle for 24 hours, and then 4 of the wells are seeded with 200ug/mL micelles and incubated overnight. After incubation, all media is removed and fresh DMEM containing no FBS is added. 60uL of 0.45um filtered 5mg/mL MTT in pure water is then added and allowed to react for 4 hours. Cell media is then carefully removed and 600uL of DMSO is added to each plate and allowed to sit for 90min. The absorption of each well is then measured to determine the cell populations' viability.

PDT/PTT Confocal Microscopy: A confocal glass bottom plate is seeded with 100,000 cells and 1mL of 200ug/mL micelles in DMEM (10% FBS, 1% Pen Strep) and incubated overnight. The cells are stained with calcein AM, washed 3 times with DPBS, and 1mL of media solution containing 10mM HEPES, 2mM $CaCl_2$, and 150mM NaCl at pH 7.4, added with 20uL of 1mg/mL PI.

Confocal imaging was performed using an ISS ALBA time-resolved confocal microscope, with an IX-81 Olympus microscope body and a U-Plan S-APO 60X 1.2NA water immersion objective. A Fianium supercontinuum laser with an acousto-optical filter was used to generate picosecond-excitation pulses at a wavelength of 488 nm at a repetition rate of 20 MHz. Fluorescent emission was separated into two channels by a 592 nm shortpass dichroic mirror and collected simultaneously through 100 um pinholes and a 531 +/- 20 nm bandpass filter (calcein channel) and a 630 ± 32 nm bandpass filter (propidium iodide channel) onto a low noise avalanche photodiode.

Photodynamic therapy was activated using a mercury arc lamp with a 692+/-20 nm excitation filter, using neutral density filters to adjust the total incident power to 50mW/cm^2. Photothermal therapy was similarly initiated using a standard ICG filter set and the power adjusted to 500mW/cm^2.

4.7 References

[1]Hopkins, T.; Folz, J.; Song, Z.; Hoff, J.D.; Kopelman, R. Multifunctional Pluronic Micelles for Targetable Photo-mediated Treatment of Choroidal Neovascularization (CNV). *Nanomedicine*, To be submitted.

[2]Zhang, D.; Wu, M.; Zeng, Y.; Wu, L.; Wang, Q.; Han, X.; Liu, X.; Liu, J. Chlorin e6 Conjugated Poly(dopamine) Nanospheres as PDT/PTT Dual-Modal Therapeutic Agents for Enhanced Cancer Therapy. *ACS Appl. Mater. Interfaces*, 2015, **7**, 8176 – 87. DOI: 10.1021/acsami.5b01027.

[3]Li, W.; Peng, J.; Tan, L.; Wu, J.; Shi, K.; Qu, Y.; Wei, X.; Qian, Z. Mild photothermal therapy/photodynamic therapy/chemotherapy of breast cancer by Lyp-1 modified Docetaxel/IR820 Co-loaded micelles. *Biomaterials*, 2016, **106**, 119 – 33. DOI: 10.016/j.biomaterials.2016.08.016.

[4]Cao, J.; Chen, D.; Huang, S.; Deng, D.; Tang, L.; Gu, Y. Multifunctional near-infrared light-triggered biodegradable micelles for chemo- and photo-thermal combination therapy. *Oncotarget.*, 2016, **7**, 82170 – 84. DOI: 10.18632/oncotarget.10320.

[5]Zhao et al. Fast-Clearable Nanocarriers Conducting Chemo/Photothermal Combination Therapy to Inhibit Recurrence of Malignant Tumors. *Small*, 2017, **13**. DOI: 10.1002/smll.201700963.

[6]Biteghe, F.N.; Davids, L.M. A combination of photodynamic therapy and chemotherapy displays a differential cytotoxic effect on human metastatic melanoma cells. *J. Photochem. Photobiol. B.* 2017, **166**, 18 – 27. DOI: 10.1016/j.jphotobiol.2016.11.004.

[7]Kimura, M.; Miyajima, K.; Kojika, M.; Kono, T.; Kato, H. Photodynamic Therapy (PDT) with Chemotherapy for Advanced Lung Cancer with Airway Stenosis. *Int. J. Mol. Sci.*, 2015, **16**, 25466 – 75. DOI: 10.3390/ijms161025466.

[8]Kopelman et al. Multifunctional nanoparticle platforms for in vivo MRI enhancement and photodynamic therapy of a rat brain cancer. *J. Magn. Magn. Mater.*, 2005, **293**, 404 – 10.

[9]Bharathiraja et al. Photo-based PDT/PTT dual model killing and imaging of cancer cells using phycocyanin-polypyrrole nanoparticles. *Eur. J. Pharm. Biopharm.*, 2017. DOI: 10.1016/j.ejpb.2017.11.007.

[10]Wang, K.; Zhang, J.; Wang, J.; Yuan, A.; Sun, M.; Wu, J.; Hu, Y. Self-assembled IR780-loaded transferrin nanoparticles as an imaging, targeting and PDT/PTT agent for cancer therapy. *Sci. Rep.*, 2016, **6**, 27421. DOI: 10.1038/srep27421.

[11]Li, Y.; Huang, D.; Xia, X.; Wang, Z.; Luo, L.; Wen, R. CCR3 and Choroidal Neovascularization. *PLoS One*, 2011, **6**, e17106. DOI: 10.1371/journal.pone.0017106.

[12]Brown, D.M.; Kaiser, P.K.; Michels, M.; Soubrane, G.; Heier, J.S.; Kim, R.Y.; Sy, J.P.; Schneider, S.; ANCHOR Study Group. Ranibizumab versus verteporfin for neovascular age-related macular degeneration. *N. Engl. J. Med.*, 2006, **355**, 1432 – 44.

[13]Kimura, H.; Yasukawa, T.; Tabata, Y.; Ogura, Y. Drug targeting to choroidal neovascularization. *Adv. Drug. Deliv. Rev.*, 2001, **52**, 79 – 91.

[14]Hah, H.J.; Kim, G.; Lee, Y.E.; Orringer, D.A.; Sagher, O.; Philbert, M.A.; Kopelman, R. Methylene blue-conjugated hydrogel nanoparticles and tumor-cell targeted photodynamic therapy. *Macromol. Biosci.*, 2011, **11**, 90 – 9. DOI: 10.1002/mabi.201000231.

[15]Gross, N.; Ranjbar, M.; Evers, C.; Hua, J.; Martin, G.; Schulze, B.; Michaelis, U.; Hansen, L.L.; Agostini, H.T. Choroidal neovascularization reduced by targeted drug delivery with cationic liposome-encapsulated paclitaxel or targeted photodynamic therapy with verteporfin encapsulated in cationic liposomes. *Mol. Vis.*, 2013, **19**, 54 – 61.

[16]Lee, C.; Folz, J.; Zhang, W.; Jo, J.; Tan, J.W.Y.; Wang, X.; Kopelman, R. Ion-Selective Nanosensor for Photoacoustic and Fluorescence Imaging of Potassium. *Anal. Chem.*, 2017, **89**, 7943 – 9. DOI: 10.1021/acs.analchem.7b00930.

[17]Kim, G.; Huang, S.W.; Day, K.C.; O'Donnell, M.; Agayan, R.R.; Day, M.A.; Kopelman, R.; Ashkenazi, S. Indocyanine-green-embedded PEBBLEs as a contrast agent for photoacoustic imaging. *J. Biomed. Opt.*, 2007, **12**, 044020. DOI: 10.1117/1.2771530.

[18]Yoon, H.J.; Lee, H.S.; Lim, J.Y.; Park, J.H. Liposomal Indocyanine Green for Enhanced Photothermal Therapy. *ACS Appl. Mater. Interfaces*, 2017, **9**, 5683 – 91. DOI: 10.1021/acsami.6b16801.

[19]Yoon, H.K.; Ray, A.; Lee, Y.E.; Kim, G.; Wang, X.; Kopelman, R. Polymer-Protein Hydrogel Nanomatrix for Stabilization of Indocyanine Green towards Targeted Fluorescence and Photoacoustic Bio-imaging. *J. Mater. Chem. B. Mater. Biol. Med.*, 2013, **1**. DOI: 10.1039/C3TB21060J.

[20]Yuan, A.; Tang, X.; Qiu, X.; Jiang, K.; Wu, J.; Hu, Y. Activatable Photodynamic destruction of cancer cells by NIR dye/photosensitizer loaded liposomes. *Chem. Commun.*, 2015, **51**, 3340 – 2. DOI: 10.1039/c4cc09689d.

[21]Melamed, J.R.; Edelstein, R.S.; Day, E.S. Elucidating the fundamental mechanisms of cell death triggered by photothermal therapy. *ACS Nano*, 2015, **9**, 6 – 11. DOI: 10.1021/acsnano.5b00021.

[22]Singh, S.R.; Grossniklaus, H.E.; Kang, S.J.; Edelhauser, H.F.; Ambati, B.K.; Kompella, U.B. Intravenous transferrin, RGD peptide and dual-targeted nanoparticles enhance anti-VEGF intraceptor gene delivery to laser-induced CNV. *Gene Ther.*, 2009, **16**, 645 – 59. DOI: 10.1038/gt.2008.185.

Chapter 5: Conclusions and Future Directions

5.1 Conclusions

PDT is a highly attractive method of dealing with biological ailments due to its ability to provide cell-specific ablation; only cells that are illuminated, and contain a PS, will experience therapeutic effects.[1] The advent of NP-mediated delivery has further heightened the cell specificity by providing a means of targeting dyes to specific biological locales and protecting them against non-specific protein adsorption/interactions.[2] In addition to this, great pains have been exercised to ensure that these materials are biologically compatible over the long term.[3] When combined with fiber optics, which have existed for over 20 years, sub-surface tumors may be easily targeted and treated.[4] However, even with these advancements, there has been little widespread adoption within the clinic. There are a number of possible reasons for this: 1) low business incentives to produce and sell due to lack of IP protection, 2) a tendency of clinicians to "stick to their guns" and thus take little notice of advancements in their field or are hesitant to adopt new methods, 3) lack of expertise in the industry to help drive adoption from work bench to work place, 4) lack of interest due to perceived shortcomings, or 5) insufficient clinical human data on how to properly apply the systems and long term data to promote FDA approval.

The pharma industry is heavily centered on being able to identify a viable market and produce a solution that generates significant profit. With respect to the above mentioned, (1) through (3) are changes that must come from within the industry. However, those changes can be influenced from the lab by providing materials that show clear cut results and efficacy that cannot be competed with when paired against traditional means of treatments in cancer (chemo,

radiation therapy, invasive surgery).[3] Therefore, the bulk of this presented work has focused on identifying the currently perceived advantages/limits of PDT methodologies and designing systems to optimize them in their specific applications, (4).

Synthesis of PAAm-Ce6 NPs helped to identify the relative PDT aggression of the classically employed dye Ce6 in NPs vs MB-NPs. In reporting this, it may be better understood in what PSs to choose for PDT based on what results a clinician may wish to see. For example, if a rapid tissue response is needed in controlling the tumor progression, then Ce6 would be an optimal choice, or if the area of operation requires a gentler treatment that favors apoptosis over necrosis to avoid inflammation (e.g. in the brain), MB would be preferable.

8PEGA has clearly presented itself as an attractive material for its biocompatibility, potential as a molecular agent in MRI, optimization in ROS production, and flexibility in targeting different ailments. In effect, 8PEGA represents a system that may be flexibly applied and optimize PDT across a variety of diseases.

Pluronic based micelles have clearly demonstrated an ability to encapsulate VP and ICG to ablate cells, enabling the potential for their targeted delivery *in vivo* to treat CNV and simultaneously avoid the issue of collateral tissue damage that is present in the current use of VP alone in the clinic. This is an important step to providing efficient treatment for a disease that is predominantly treated by intravitreal delivery of antigrowth factors, which only treat the condition as opposed to stopping it.

It is hoped that the reported data here may further drive interest to clinically adopt NP-mediated PDT as a methodology in surface/sub-surface cancer and cancer-like diseases.

5.2 Future Directions

Having shown in cell work the efficacy for the above systems (F3-8PEGA-Ce6 and VP/ICG pluronic micelles), they should now be translated to animal models. Specifically, the F3-8PEGA-Ce6 animal work should focus on demonstrating accumulation in and imaging of tumor tissue, as well as determining renal clearance of animals. VP/ICG micelles will be used in rabbit models where CNV has been artificially induced to demonstrate their efficacy, selective accumulation, and ablation of the anomalous vasculature. A combination of fluorescence, photo-acoustic, or optical computational topography images will be used to visualize the effects and progression of the condition with PDT treatment.

It is believed that further optimization of the NPs presented above would also be accomplished by using long wavelength NIR dyes. In addition, establishing preferred protocols of PDT application in non-xenograft models will be necessary to allow proper patient treatment.

5.2.1 PS Selection and Design

With respect to PS design for PDT, porphyrins are commonly used a base material in synthetic investigation due to their excellent ROS production properties. However, there has not been a significant number of reported derivatives with successful shifting of excitation and emission deep into the NIR. One current example would be TOOKAD Soluble (Figure 5-1).[5]

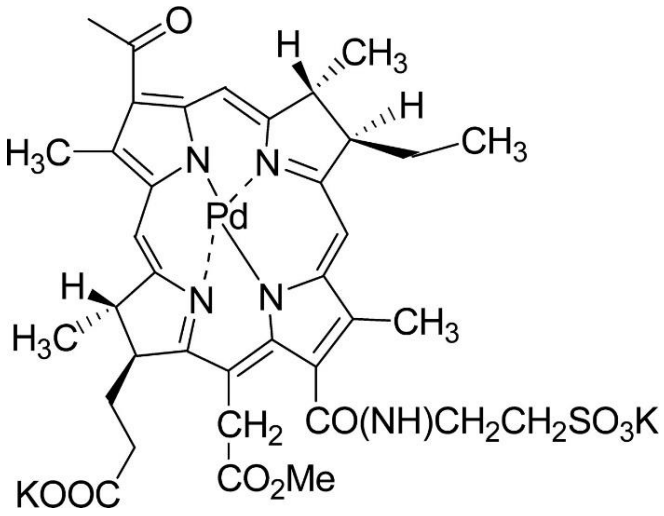

Figure 5-1: TOOKAD Soluble structure. Lambda max = ~763nm. Reproduced from reference 5.

Notably, TOOKAD Soluble contains a coordinated palladium atom. Coordinating metals have been thoroughly explored in the literature for increasing ROS production through the heavy atom effect.[6]

It has been reported in Dr. Ravindra K. Pandey's book "Handbook of Photodynamic Therapy" that the resonance wavelength of porphyrins can also be influenced through modification of the central porphyrin ring.[7] This has been substantiated in the literature[8,9] and has even been investigated using ring expansions that contain hetero atoms, like sulfur.[10] Good ROS production has been shown for these structures.[11] It is therefore believed that work should be done on finding a careful balance of porphyrin ring expansion, heteroatom replacement, coordinating metals, and R group choice to tune the absorption, solubility, and ROS generation properties to sufficiently enhance efficacy of porphyrin PSs for subsurface tumor PDT treatment.

5.2.2 Understanding Biological Complexity involved in Applying PDT

Currently, enabling PDT treatment of sub-surface tumors is possible even without deep NIR absorbing PSs, as fiber optics can easily provide the necessary light to many body locations.[3] A very important issue is dealing with case-by-case differences of how tumors grow, proliferate, and consume their nutrients. This specifically refers to how, in each patient, a tumor may be of different size, shape, chemical content or location (relative to vasculature and biological environment). For example, a tumor that is highly networked in the tissue may be less prone to hypoxia when compared to one that is a single large mass. Therefore, future studies should place emphasis on the general shape and location and oxygen content of a tumor, to optimize how best the PDT should be applied; creating a library of data on examined tumor models and measuring their levels of hypoxia photo-acoustically would be highly beneficial.

There are three potential methods of suitably applying PDT: 1) sequential administration of PDT to progressively shave down the tumor mass, 2) increasing tissue oxygenation (whether by additives that increase tissue oxygenation like sodium salt transcrocetin[12] or breathing oxygen rich air), or 3) coupling with PTT.

Combinations of any of these three methods may be advantageous. For example, a tumor that is a single large mass may require sequential doses of PDT to completely remove it (each dose would expose sub-layers of the tumor, which would subsequently re-oxygenate). But, fewer subsequent doses may be needed and faster total ablation accomplished with heightened oxygenation. Likewise, PTT may remove the limitation of low oxygen deeper within the tumor mass, due to its effect being independent of oxygen concentration, but may also be limited based on the biological environment; PTT classically induces necrosis, leading to inflammation of tissue that would be better avoided in certain areas, like the brain.

Thus, future work on the evaluation of best practices and application methods is exceptionally important. This should encompass using any one of the three above approaches singularly or applying them in any combination and studying how the responses are correlated.

5.3 References

[1]Avula et al. Cell-selective Arrhythmia Ablation for Photomodulation of Heart Rhythm. *Sci. Trans. Med.*, 2015, **7**, 311ra172. DOI: 10.1126/scitranslmed.aab3665.

[2]Kopelman et al. Multifunctional nanoparticle platforms for in vivo MRI enhancement and photodynamic therapy of a rat brain cancer. *J. Magn. Magn. Mater.*, 2005, **293**, 404 – 10.

[3]Lai, W.; Hu, Z.; Fang, Q. The Concerns on Biosafety of Nanomaterials. *JSM Nanotechnol. Nanomed.*, 2013, **1**, 1009.

[4]Agostinis et al. PHOTODYNAMIC THERAPY OF CANCER: AN UPDATE. *CA Cancer J. Clin.*, 2011, **61**, 250 – 81. DOI: 10.3322/caac.20114.

[5]Betrouni, N.; Noukris, S.; Benzaghou, F. Vascular targeted photodynamic therapy with TOOKAD® Soluble (WST11) in localized prostate cancer: efficiency of automatic pre-treatment planning. *Laser Med. Sci.*, 2017, **32**, 1301 – 7. DOI: 10.1007/s10103-017-2241-7.

[6]Stacey, O.; Pope, S.J.A. New avenues in the design and potential application of metal complexes for photodynamic therapy. *RSC Adv.*, 2013, **3**, 25550. DOI: 10.1039/c3ra45219k.

[7]Pandey, R.K.; Kessel, D.; Dougherty, T.J. *Handbook of Photodynamic Therapy: Updates on recent Applications of Porphyrin-Based Compounds.* World Scientific: To Tuck Link, 2016.

[8]Chatterjee, T.; Shetti, V.S.; Sharma, R.; Ravikanth, M. Heteroatom-Containing Porphyrin Analogues. *Chem. Rev.*, 2017, **117**, 3254 – 328. DOI: 10.1021/acs.chemrev.6b00496.

[9]Xu, H.; Mack, J.; Wu, D.; Xue, Z.; Descalzon, A.B.; Rurack, K.; Kobayashi, N.; Shen, Z. Synthesis and Properties of Fused-Ring-Expanded Porphyrins that were Core-Modified with Group 16 Heteroatoms. *Chem. Eur. L.*,2012, **18**, 16844 – 67. DOI: 10.1002/chem.201200956.

[10]Chandrashekar, T.K.; Prabhuraja, V.; Gokulnath, S.; Sabarinathan, R.; Srinivasan, A. Fused core-modified *meso*-aryl expanded porphyrins. *Chem Commun.*, 2010, **46**, 5915 – 7. DOI: 10.1039/c000387.

[11]Hilmey et al. Water-Soluble, Core-Modified Porphyrins as Novel, Longer-Wavelength-Absorbing Sensitizers for Photodynamic Therapy. II. Effects of Core Heteroatoms and Meso-Substituents on Biological Activity. *J. Med. Chem.*, 2002, **45**, 449 – 61. DOI: 10.1021/jm0103662.

[12]Gainer, J.L. Trans-sodium-crocetinate for treating hypoxia/ischemia. *Expert Opin. Investig. Drugs*, 2008, **17**, 917 – 24. DOI: 10.1517/13543784.17.6.917.